Alma Mater Studiorum · Università di Bologna

Scuola di Scienze
Dipartimento di Fisica e Astronomia
Corso di Laurea in Fisica

Analysis of the Performance of DT Trigger Algorithms for the Phase-2 Upgrade of the CMS Detector

Relatore:
Prof. Luigi Guiducci

Correlatore:
Dott. Carlo Battilana

Presentata da:
Francesco Vascelli

Anno Accademico 2018/2019

Abstract

In questa tesi sono state studiate le prestazioni di due nuovi algoritmi per il trigger locale delle camere a deriva dell'esperimento CMS (*Compact Muon Solenoid*). Gli algoritmi sono stati sviluppati in vista dell'upgrade del collisionatore LHC (*Large Hadron Collider*), che diventerà High Luminosity LHC, e del corrispettivo upgrade di CMS. In particolare, sono stati svolti studi sull'efficienza degli algoritmi e si sono analizzati i casi in cui più segmenti di trigger vengono prodotti per un singolo muone che attraversa una camera del rivelatore. Le prestazioni dei nuovi algoritmi sono anche state comparate con quelle del sistema di trigger attualmente in uso.

Questo lavoro è stato realizzato sviluppando uno strumento di analisi che sfrutta il pacchetto software di ROOT. I dati processati provengono da simulazioni nelle quali sono generate isotropicamente coppie di muoni con un'energia tra 2 e 100 GeV. Inoltre, vengono confrontate generazioni di muoni senza pile-up e con un pile-up medio di 200 collisioni per evento.

Contents

Introduction

The Large Hadron Collider (LHC) is a particle accelerator operating at CERN (Geneva). This collider is able to provide proton-proton interactions at a center-of-mass energy of 13 TeV and reaches values of instantaneous luminosity up to $2 \times 10^{34} \mathrm{cm}^{-2}\mathrm{s}^{-1}$. The Compact Muon Solenoid (CMS) is a multipurpose detector operating at LHC. The outermost part of CMS is equipped with a muon system, consisting of three different types of gas ionization chambers arranged in multiple layers to record a muon track path at different points. The CMS muon system ensures efficient identification of muon and provides trigger capabilities, including the ability to identify the bunch crossing of origin of in coming muons, and measure their transverse momentum. In the CMS barrel region of the muon system, Drift Tubes Chambers (DT) serve both as offline tracking and triggering detectors. The Drift Tubes local trigger logic is able to identify the parent bunch crossing of an incoming muon track and to measure its position and direction within a chamber. To extend the sensitivity for new physics searches, a major upgrade of the LHC is being prepared, the High Luminosity LHC (HL- LHC). In the upgraded collider, the interaction center-of-mass energy will reach 14 TeV and the peak instantaneous luminosity will increase up to $7.5 \times 10^{34} \mathrm{cm}^{-2}\mathrm{s}^{-1}$. A systemic upgrade of the CMS detector, labeled Phase-2 upgrade, is needed to maintain high physics performance under the harsh HL-LHC conditions. In particular, new chambers will be installed in the forward region of the muon system, and most of the electronics of the muon spectrometer will be replaced. In the case of the DT, the electronic upgrade will allow to deploy a more refined local trigger logic, which is expected to outperform the existing one. This work focuses on the studies of new algorithms for the barrel muon local trigger of the DT Chambers proposed for the Phase-2 upgrade. The goal is to compare the present Phase-1 algorithm with two new algorithms proposed for Phase-2, in terms of performance. For this analysis, the efficiency of the new algorithms is measured and compared with the one of the present (Phase-1) trigger. Similarly, the events where a single crossing muon generates multiple triggers in a given DT chamber (ghosts) are studied both for the Phase-2 and Phase-1 DT local triggers. Samples of simulated muons, produced either with no overlapping pile-up collisions or combined with an average of 200 collisions per bunch crossing, are used.

In chapter 1 the LHC apparatus and the CMS detector are presented, with the main focus on Drift Tubes Chambers. In chapter 2 the CMS trigger system is described, along with a general presentation of the Phase-2 DT detector upgrade and of the Phase-2 local trigger algorithms. Finally, in chapter 3, a study of the performance of the Phase-1 and Phase-2 DT local trigger algorithms, in terms of efficiency and fraction of ghosts, is presented.

Chapter 1

LHC and the CMS Experiment

1.1 The Large Hadron Collider

The Large Hadron Collider (LHC) is an accelerator machine built between 2002 and 2010 by the European Organization for Nuclear Research (CERN) and placed in a 27 km long undergroung circular tunnel near Geneva. LHC can accelerate protons up to a center-of-mass energy of 13 TeV and heavy-ions up to a center-of-mass energy of 2.76 TeV per nucleon pair.

The two proton beams run in separate beam pipes. In order to keep them in a approximately circular orbit, their trajectory is bent using compact twin-bore superconducting magnets reaching a magnetic field of 8.3 T, cooled at 2.1 K with superfluid helium. The beams have a bunched structure (about $N = 1.1 \times 10^{11}$ protons per bunch) with a bunch crossing (BX) frequency of $f = 40$ MHz, corresponding to a time between collisions of $\tau = 25$ ns.

The proton injection is done employing pre-existing accelerators, comprising the Linac (Linear Accelerator), the PSB (Proton Synchrotron Booster), the PS (Proton Synchrotron), and the SPS (Super Proton Synchrotron). Given all these steps an injection energy at LHC of 450 GeV is reached. The LHC beam filling requires about two hours. The beam lifetime is about 22 hours, however the data are usually taken only in the first 10 hours, then the beams are dumped and a new filling is started in order to restart at maximum beam intensity to maximize the integrated luminosity collected by the detectors.

There are four interaction points, where detectors are located: ATLAS (A Toroidal LHC ApparatuS) and CMS (Compact Muon Solenoid) are general purpose detectors, ALICE (A Large Ion Collider Experiment) focuses on the heavy ions physics and on the study of the quark-gluon plasma, and LHCb (LHC beauty experiment) studies the CP violation in b-physics (Fig. 1.1)

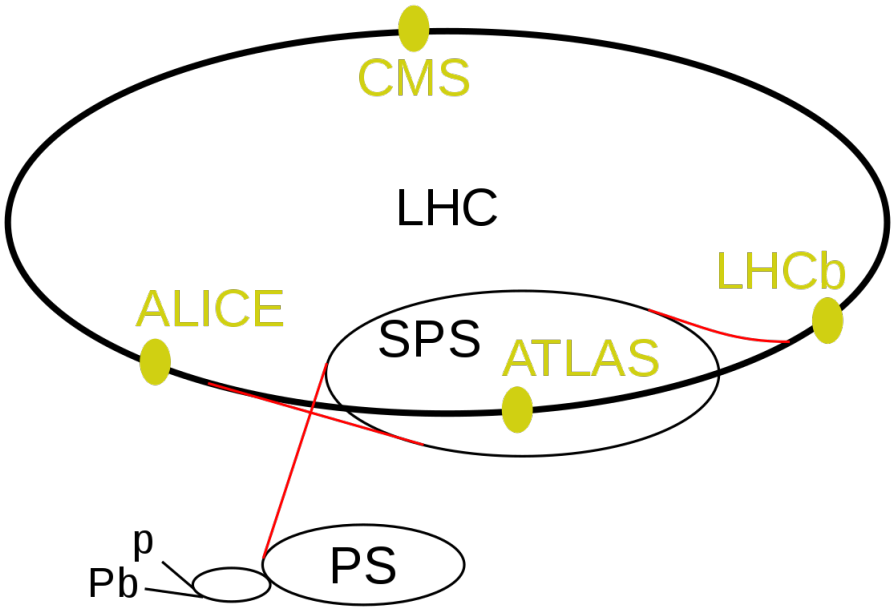

Figure 1.1: The CERN accelerator complex and the interaction points of the main LHC experiments

1.2 The Compact Muon Solenoid

The Compact Muon Solenoid (CMS) [1] is a multipurpose detector 21.6 m long, with a diameter of 15 m and a weight of about 12500 tons. A high quality tracking system allows track reconstruction with very high spatial resolution his located at its center. It is surrounded by electromagnetic and hadron calorimeters, which perform energy measurements on electrons, photons and hadrons coming from jets. Outside the calorimeters, a superconducting solenoid generates a magnetic field up to 3.8 T inside the its volume, in order to provide large bending power. The field outside the solenoid is strong enough to saturate the iron return yoke where a complex muon spectrometer is placed. The spectrometer is composed by a cylindrical barrel, segmented in five wheels, and two endcaps, built of four disks each. It is based on four layers of Drift Tubes detectors and Cathode Strip Chambers, respectively positioned in barrel and endcaps. Resistive Plate Chambers complement the other muon subdetectors ensuring redundancy and improving trigger capabilities. A slice of the CMS detector is presented in Fig. 1.2.

In CMS, a right handed coordinate system is defined, centered at the nominal collision point: the x-axis points radially inward to the center of the accelerator ring, the y-axis points upward and the z- axis is parallel to the beam pipe. The azimuthal angle ϕ is measured in the x-y plane in a $0 < \phi < 2\pi$ range, while the polar angle θ is measured from the z-axis using a $0 < \theta < \pi$ range. Usually the polar angle θ is replaced by the pseudorapidity η defined as:

$$\eta = -\ln\left(\tan\frac{\theta}{2}\right)$$

Another important and useful quantity is the 3-momentum component perpendicular to the beam z-axis, called transverse momentum p_T defined as:

$$p_T = \sqrt{{p_x}^2 + {p_y}^2}$$

where p_x and p_y are the x and y components of the 3-momentum in the ϕ-plane, perpendicular to the beam axis.

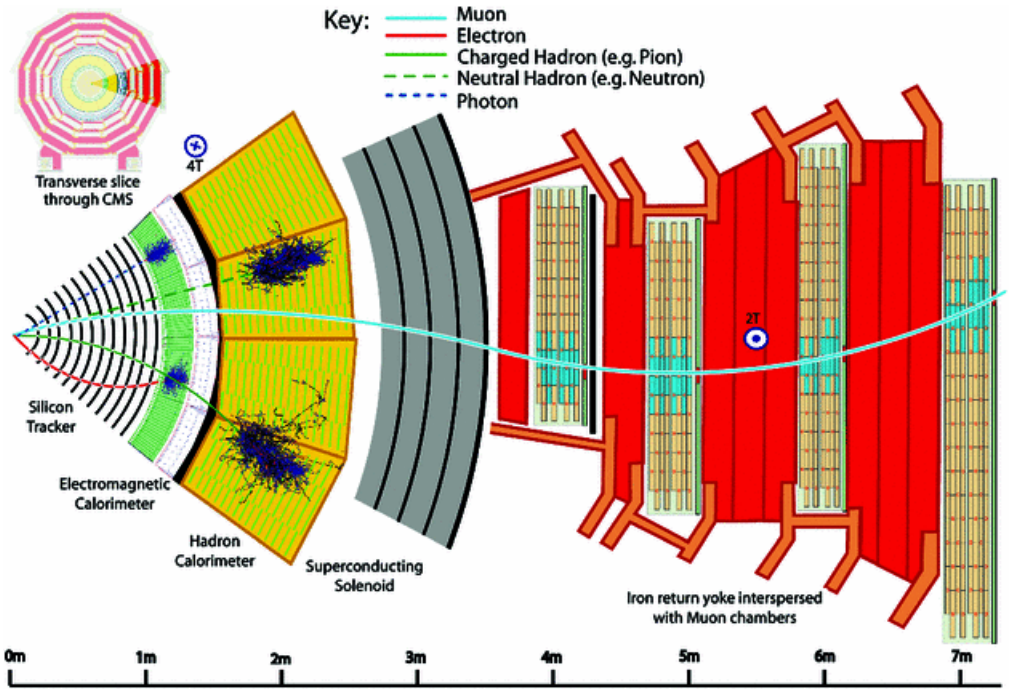

Figure 1.2: A transverse slice of the Compact Muon Solenoid.

1.3 Muon Detector Structure

CMS uses three types of muon detectors [2]: Drift Tubes (DT), Cathode Strip Chambers (CSC), and Resistive Plate Chambers (RPC). DTs are designed to carry out precise trajectory measurement and are placed in the central barrel region ($\eta < 1.2$) characterized by low occupancy, low background, and low residual magnetic field. CSCs are used in the end caps ($0.9 < \eta < 2.4$), where the background rate is higher and magnetic field is less uniform. RPCs provide a fast signal when a muon crosses the muon detector, and they are installed in both the barrel and the end caps ($\eta < 1.8$). A longitudinal view of the CMS muon detector is presented in Fig. 1.3.

The DT system (Fig. 1.4) is segmented in 5 wheels along the z direction, each about 2.5 m wide and divided into 12 azimuthal sectors, covering about 30° each. Drift Tubes Chambers are arranged in 4 concentric cylinders, called stations, at different distances from the interaction point and interleaved with the iron of the yoke. Each DT station consists of 12 chambers in each wheel, with the exception of the outermost station MB4, whose top and bottom sectors are equipped of one more chamber each (sector 13 and 14 respectively), thus yielding a total of 14 chambers in that station. Each DT chamber is azimutally staggered with respect to the preceding inner one, in order to maximize the geometrical acceptance.

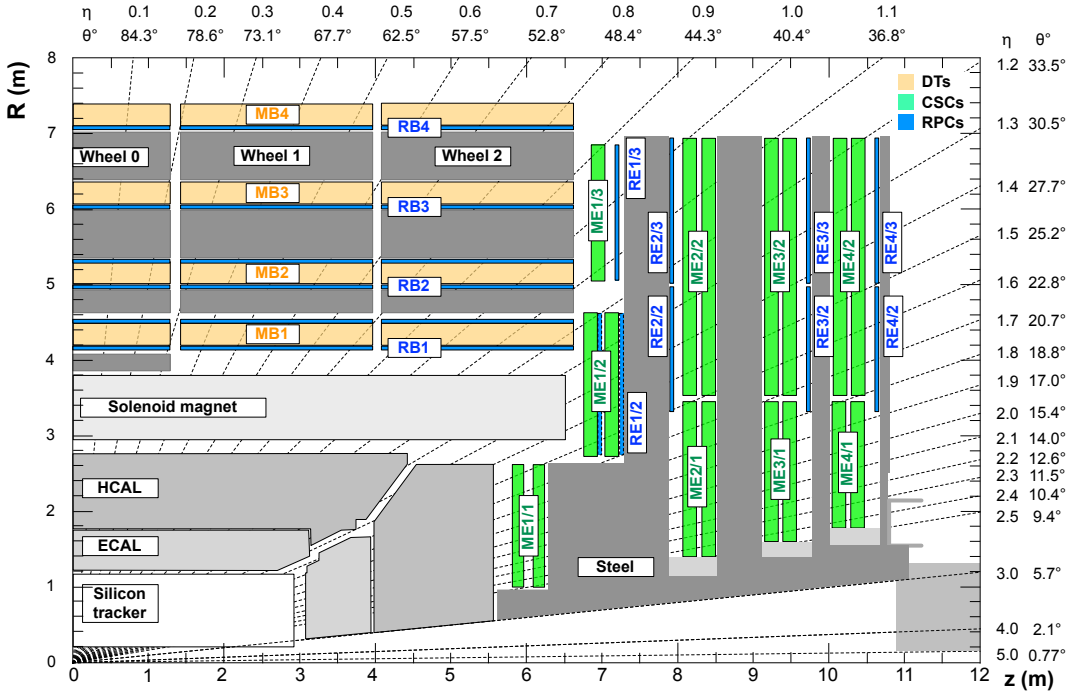

Figure 1.3: CMS muon system tranverse view.

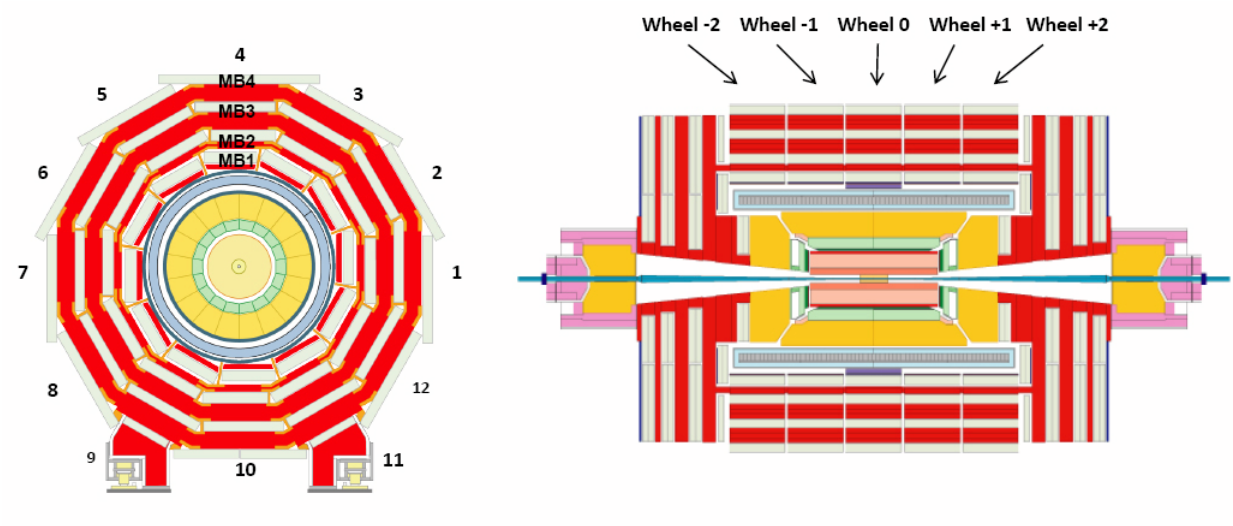

Figure 1.4: CMS detector longitudinal (left) and transverse (right) views.

1.4 Drift Tube Chambers

DT chambers are used in the barrel of the CMS muon system and their dimension are variable, depending by constraints coming from wheel and sector segmentation. One single chamber is composed by multiple layers of drift cells, arranged to measure position in the ϕ-view and along the z axis. Groups of four layers, staggered of half cell, form a single detection superlayer (SL). Three separate layers are enough to allow segment identification within a SL, however a fourth layer guarantees redundancy to reconstruction algorithms and to the local trigger system. DT chambers of the MB1/2/3 stations are composed of three SLs, two of them devoted to the measurement of position in the r-ϕ plane, the other being used to measure the z coordinate. To precisely measure a curved track trajectory in the azimuthal plane, detection of the ϕ-view direction is needed. In order to increase the level-arm between the two detection planes, hence improve the angular resolution within a chamber, the two r-ϕ SLs are separated by an aluminium honeycomb plate. The trajectory in the η-view is, instead, supposed to be a straight line, therefore a single SL of detection is enough to achieve the needed precision along z. Moreover MB4 chambers are not equipped with a η-view SL and consist only of the two r-ϕ SLs. The goal of the mechanical construction of a chamber is to achieve a spatial resolution for locally reconstructed segments of 100/150 μm in the r-ϕ plane measurement and a time resolution of $\sim$2 ns.

The basic detector element of the DT muon system is a Drift Tube cell of transverse dimensions 42 mm $\times$ 13 mm, whose section is shown in Figure 1.5. Each cell is filled with gas and has a stainless steel anode wire in the middle, with diameter 50 µm and length varying from 2 to 3 m. A layer of cells is obtained by two parallel aluminum

planes within which a series of "I"-shaped aluminum beams (1.2 mm thick and 9.6 mm high) define the boundaries among adjacent cells. Aluminum strips, deposited on both faces of each I-beam and electrically isolated from the I-beam body using Mylar tape, serve as cathodes. Anode wires and cathode strips are put at positive and negative voltage respectively, and provide the electric field within the cell volume. A muon (or any charged particle) crossing the cell ionizes the gas within it, releasing electrons that will move accordingly to the electric field, that is towards the anode wire. This signal is amplified proportionally to the electric potential difference ΔV between the wire and the strip, and generates an electron avalanche that produces a current on the wire.

The signal is then amplified and discriminated by the Front-End (FE) electronics for further time digitization: a threshold voltage of 20 mV is needed. The distance of the traversing track to the wire is thus measured by the drift time of ionization electrons. To provide additional field shaping to improve the space-to-distance linearity over the cell, two additional positively-biased strips are mounted on the aluminum planes (with an insulator in between) on both inner surfaces in the center of the cell itself, just in correspondence of the anode wire. Nominal voltages are +3600 , +1800 V and -1200 V for wires, strips, and cathodes respectively. The cells are filled with a 85%/15% gas mixture of Ar/CO_2, which provides good quenching properties and saturated drift velocity with a value of $v_{drift} \approx 54$ µm/ns. Thus, a maximum drift time (half-cell drift distance) of $\sim$400 ns is obtained.

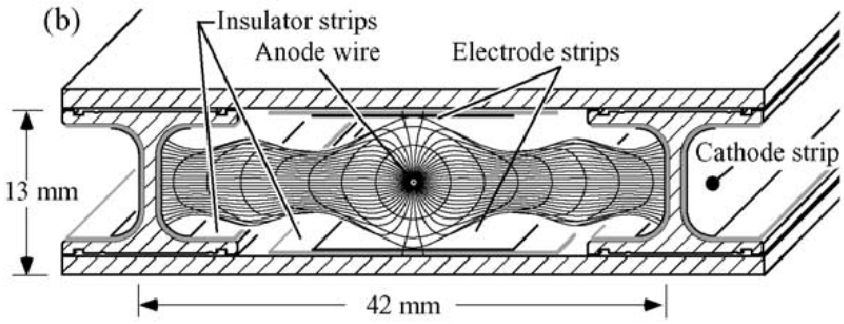

Figure 1.5: A transverse section of a Drift Tube cell

Chapter 2

Muon Trigger and Phase-2 algorithms

At LHC proton bunches collide every 25 ns. At the peak luminosity of $2\times10^{34}\text{cm}^{-2}\text{s}^{-1}$ the proton-proton interaction rate exceeds 1 GHz. Only a small fraction of these collisions can be stored for later offline analysis, and the selection must e based on the CMS physics program. This selection task is performed by the trigger system. The trigger system is expected to be able to select only the interesting events for offline storage from the bulk of the inelastic collision events.

The trigger system operates in two main steps [3]. The Level-1 trigger (L1T) is based on custom electronics, and has to reduce the number of accepted events down to a maximum rate of 100 kHz. After this stage, each event can take much more time for its processing, since the bandwidth has been already reduced and events are processed in parallel by different machines of the High Level Trigger (HLT). The HLT consists in a streamlined version of the CMS offline reconstruction, running on a filter farm of about a thousand of commercial processors.

2.1 The Level-1 Trigger System

The Level-1 trigger [4] must cope with the machine bunch crossing (BX) frequency of 40 MHz and the time between collisions is far too short for running any kind of non trivial algorithm and for taking a decision on accepting that event. However complete information from the subdetectors is stored in First In First Out (FIFO) memories. In parallel, the trigger logic runs using a subset of the information, pipelined in small steps requiring less than 25 ns each, in order to start a new event processing every BX, even if the full processing requires a much longer time to complete. At the end of the logic chain a decision is taken. If the event has to be kept, the FIFO memories containing the detector data are read and sent to the HLT. The maximum time available for the trigger

logic to take a decision is determined by the amount of BXs for which the detector data can be stored into FIFOs, and corresponds to 3.4 μs.

2.1.1 The Phase-1 Level-1 Muon Trigger System

The CMS experiment is instrumented with three muon subdetectors with a different $|\eta|$ coverage and different time and space resolution capabilities. The present L1 Muon Trigger (called Phase-1 Muon Trigger) is designed to exploit the subdetector redundancy at an early stage to improve the overall performance. For this reason, the system is composed of three separate muon track finders covering different η regions. The barrel muon track finder (BMTF) receives data from drift tube (DT) and resistive plate chamber (RPC) detectors, and covers the $|\eta| < 0.83$ region. The endcap muon track finder (EMTF) receives data from RPC and cathode strip chambers (CSC) in the region $|\eta| > 1.24$. Finally, the overlap muon track finder (OMTF) receives data from the three subdetectors in the intermediate region $0.83 < |\eta| < 1.24$. The output of the three systems is collected by the Global Muon Trigger (GMT) which ranks the muons by transverse momentum and quality, and removes the reconstruction duplicates across boundary regions. This study is focused on the barrel region of the muon trigger, which is described in the following sections.

2.2 DT Local Trigger

The goal of the DT Local Trigger system is the detection of charged particles crossing the muon barrel chambers. It has to measure position and trajectory of the crossing particles, as well as to identify their origin in terms of BX. It also associates to the reconstructed segments a quality word based on the numbers of layers involved in the measurement. Each DT chamber is equipped with a so called "minicrate" containing the local trigger and readout electronics. As shown in Fig. 2.1, the signals coming from single DT cell wires are initially processed by Bunch and Track identifiers (BTIs) that operate rough track fitting within a single SL and perform BX assignment. In a second step the Track Correlators (TRACOs) are devoted to matching the information coming from the two ϕ-SLs at the same BX and improve the parameter measurements. Then the Trigger Server (TS) performs a quality based selection on the segments coming from different TRACOs. Finally, information from different chambers within a sector are forwarded to the TwinMux Barrel Concentrator Board that has to merge and combine information coming not only from DT but also from RPC and Hadronic Calorimeter.

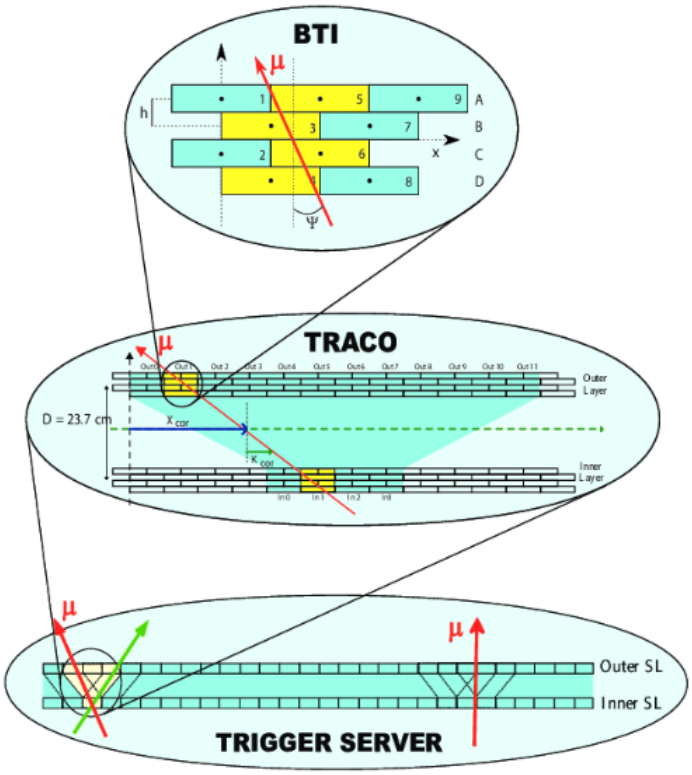

Figure 2.1: Block scheme of the DT local trigger architecture

2.2.1 Bunch and Track Identifier

The BTI is the DT trigger front-end device and has the task to associate a track segment to a charged particle crossing a SL. The track segment identification is performed exploiting the mean-timer property [5], that allows the track BX to be computed for every combination of track hits from 3 different cells The presence of a fourth layer improves the system redundancy and robustness. Furthermore on the basis of redundancy is also possible to perform a distinction between "High" and "Low" quality segments, respectively obtained by four or three aligned hits matched in a single SL. Each BTI is connected to 9 cells of a single SL and adjacent BTIs partially overlap in order to avoid geometrical inefficiencies. BTIs are identical in both the ψ-view and θ-view SLs and their number per SL only depends on the chamber size.

2.2.2 Track Correlator and Trigger Server

The Track Correlator (TRACO) is the second element of the DT Local Trigger chain and it is devoted to the association, within a muon chamber, of the track segments delivered by predefined groups of BTIs belonging to the two ϕ-superlayers. It attempts correlation between BTI segments coming from inner and outer SLs and links the information between the two, improving track parameters determination. Each TRACO can then send up to two candidates to the Trigger Server for further processing.

The Trigger Server (TS) is the last on-board component of the DT Local Trigger logic and has the task to select the two best trigger candidates (in terms of quality and p_T) among the track segments selected by all the TRACOs and to send them out of the minicrate.

2.3 TwinMux and Barrel Muon Track Finder

Within the CMS Phase-1 trigger, the TwinMux is the adaptive layer for the track finder in the barrel region. To cover the full area, 60 TwinMux boards are hosted. They merge information from DT and RPC and forward data to the Barrel Muon Track Finder (BMTF) applying a scale up in the transmission rate and a reduction in the number of links. The TwinMux system is also responsible for duplicating data (up to four times for the sectors of the outer wheels where data are shared between barrel and overlap track finders) in order to reduce connections between trigger processors increasing the reliability of the system.

Each TwinMux receives DT and RPC links from one sector of the barrel muon detector. The data coming from these two sub-systems contain different informations: Trigger Primitives sent from DTs include position, direction, quality, and BX information whereas hits coming from RPCs include position and BX information only. DT and RPC data are combined, if possible, improving the local trigger response. Once such combined primitives have been produced they are sent to the BMTF that reconstructs muon track candidates exploiting a Kalman Filter based algorithm.

2.4 Phase-2 Detector Upgrades

The High Luminosity LHC (HL-LHC) is an upgrade of the LHC to achieve larger instantaneous luminosity, thereby enabling the experiments to enlarge their data sample by one order of magnitude compared with the LHC baseline program [6]. The CMS upgrade program, called Phase-2 upgrade [7] is therefore crucial to enable operation on the collider beyond 2025. The brightness of beams and the new focusing/crossing scheme at the interaction point will enable the accelerator to operate at a peak luminosity of $7.5 \times 10^{34} \mathrm{cm}^{-2}\mathrm{s}^{-1}$, corresponding to a mean pileup of 200 interactions per beam crossing.

The primary goal of the Phase-2 upgrade program is therefore to maintain the excellent performance in terms of efficiency, resolution, and background rejection, of the CMS Phase-1 detector, under these challenging conditions. The main challenges that must be overcome to achieve this goal are radiation damage to the CMS detector from the large integrated luminosity, and the very high pileup that comes from the high number of interactions per beam crossing.

The Tracker will suffer significant radiation damage and must be completely replaced for Phase-2. For Phase-2 operation, the total latency will be increased to 12.5 μs to provide sufficient time for the hardware track reconstruction and matching of tracks to muons and calorimeter information in the L1 trigger. This change will require upgrades of the readout electronics in some of the existing sub-detectors that will be kept for Phase-2. Based on the expected performance of the trigger with track information, the proposed L1 trigger acceptance rate is 500 kHz: this will allow CMS to maintain a physics yeld comparable to the typically delivered during the last LHC run. It is important for Phase-2 physics to keep the efficiency of the L1 muon triggers high, while maintaining p_T thresholds low enough to collect a large fraction of Higgs, top quark, and electroweak bosons.

In preparation for the HL-LHC, DT plans [8] are focused on system longevity and related upgrades in the electronics. No intervention is foreseen on the chambers themselves, but measures are being taken to reduce the expected degradation. Instead, a full replacement of on-detectors and off-detectors electronics is foreseen.

Present minicrates (one per DT chamber) host the time digitization logic and the complex logic for the L1 trigger primitive generation. The survival of this system is not guaranteed in the harsh HL-LHC environment and it is incompatible with increasing the Level-1 trigger acceptance rate beyond 300 kHz. Consequently, the substitution of this electronics is planned. For simplicity and ease of maintenance, the new minicrates will only implement the time digitization and control functions, moving the complex trigger logic to the service cavern. The current implementation of the DT electronics introduces significant limitations to the maximum readout rate and severely constrains the trigger primitive algorithms due to it's low input sampling frequency (80 MHz). Therefore, a higher bandwidth is needed and it is easily achievable at low cost using current optical link technologies. The replacement is expected to allow the implementation of full time (and therefore space) resolution and to provide complete chamber information in the DT trigger system, with improved performance in terms of rate reduction and better matching with the tracker at the Level-1 trigger.

In the Phase-2 upgrade, the trigger primitive generation and the readout event matching will be performed in the underground control room on generic hardware, based on the latest commercial FPGAs. New trigger primitives will have a direction and position resolution closer to those of present HLT reconstructed segments. Studies are needed to define the algorithm that provides the best improvement at a reasonable implementation cost.

2.5 Algorithms for the Phase-2 DT Local Trigger

Two algorithms are presently being evaluated as candidates to perform DT Trigger Primitive (TP) generation. Both are implemented in software (as C++ emulators) and validated in real hardware demonstrators. They assume that muons follow a straight path inside a chamber and rely on the mean-timer property, holding for triplets of half staggered drift cells characterized by constant drift velocity, that allows the bunch-crossing of origin of an incoming muon to be identified.

2.5.1 Analytical Method

The first algorithm, called Analytical Method (AM), has been designed following a very direct hardware oriented approach [9]. It operates in three steps, called grouping, fitting and correlation.

Starting from a group of 10 nearby cells distributed across the four layers of a DT SL, the grouping step selects patterns of 3 or 4 fired DT cells compatible with a straight line.

From those patterns, the fitting step exploits the mean-timer property to compute unambiguously the BX corresponding to every subset of 3 cells within each pattern. For cases with 4-cells patterns, the BX of each triplet is combined with the others using an arithmetic mean. Track parameters are then computed using exact formulas from χ^2 minimization.

Finally, a correlation between the two $R-\phi$ SLs is attempted. A potential match between the primitives of the SLs in the same chamber is looked for, within a window of ± 25 ns. If a match is found, the track parameters are recalculated, either as an arithmetic mean of the ones of each SL (position, time), or as ratio of the difference between the positions of each primitive and the distance between the two SLs (direction). If no match is found, all per-SL primitives are forwarded to the next stage to maintain high efficiency.

2.5.2 Histogram-Based

The second algorithm, called Histogram-Based (HB) method [10], operates BX identification using a histogram-based mean-timer technique (called Majority Mean-Timer, MMT) and performs track segment reconstruction using a Compact Hough Transform (CHT) method.

In MMT, all meaningful triplets in a set of pre-clustered channels (called a macrocell) are used to identify the muon bunch-crossing by exploiting the mean-timer property. The most voted result among all triplets is chosen as candidate BX within a given macrocell. Votes are filtered, before being counted, in case they are compatible with a meaningful quadruplet pattern.

Within the CHT, all permutations of TDC count pairs from different layers are processed in parallel to compute track slope hypotheses. Three histograms, two with pairs from each $R-\phi$ SL and one from pairs built using both $R-\phi$ SLs, are filled with such hypotheses. The results are combined, after applying a threshold cut, and the most voted hypothesis, common to all histograms, is chosen as track slope for the TP. The TPs track intercept position is then calculated out of the, already computed, crossing time and track slope, after converting TDC counts into spatial coordinates.

2.6 Phase-1 and Phase-2 Local Trigger Qualities

In both Phase-1 and Phase-2 algorithms, the multiplicity and permutation of hits used to build a TP define the trigger segment quality. Highest quality TPs are the ones where patterns of 3 or 4 hits from both $R-\phi$ SLs are exploited to assess the BX and get combined in a single TP (correlated triggers). Alternatively, the BX can be identified and a TP can be built out of 3 or 4 hits from only one SL (uncorrelated triggers). In the case of Phase-2 algorithms, one or two hits from the second $R-\phi$ SL may be used to confirm and improve a trigger segment for uncorrelated triggers. These confirmed triggers get also flagged with dedicated qualities. In Tab. 2.1, both Phase-1 and Phase-2 qualities are described. The new algorithms proposed for Phase-2 provide an expansion of the trigger primitives qualities with respect to the Phase-1 definitions, where the configuration "+2" is absent.

Phase-1 code	**AM code**	**HB code**	**Quality label**	**Meaning**
6	9	9	4+4	Correlated H+H trigger
5	8	8	4+3	Correlated H+L or L+H trigger
/	7	7	4+2	(4+2)/8 hits trigger
4	6	6	3+3	Correlated L+L trigger
/	5	5	3+2	(3+2)/8 hits trigger
3 - 2	4 - 3	4	4/4	Uncorrelated H trigger
1-0	2 - 1	3	3/4	Uncorrelated L trigger

Table 2.1: Correspondence between Phase-1 , AM and HB coding for each quality label.

Chapter 3

Performance of DT Local Trigger Algorithms

The goal of the analysis presented in this chapter is to compare the performance of the Phase-1 DT Local Trigger algorithm with the ones proposed for the Phase-2 upgrade, described in the previous chapter (AM, HB). The trigger performance could be studied through many figures, such as efficiency, spatial and time resolution, effect of pile-up, resilience to detector aging or rate of spurious tracks. In this work, the metrics used to evaluate performance are the local DT trigger efficiency, computed with respect to offline reconstruction, and the fraction of cases where multiple copies of a trigger are reconstructed within a chamber traversed by a single muon (ghosts). In time ghosts can affect the muon trigger performance, by producing, for instance, more track hypotheses at the track finders, which can result in a wrong estimate of the transverse momentum or the misidentification of single muon events as dimuon ones. Ghosts at a different BXes could result in a wrong BX assignment of the track finder candidates, which may cause the loss of the event.

To perform this study, samples of simulated data are used. These samples consist of $N = 100,000$ events. For each event two back-to-back muons with a transverse momentum in the range between 2 and 100 GeV are generated. Each muon is produced isotropically in the x-y plane ($-\pi \leq \phi \leq \pi$) and with a pseudorapidity $|\eta| < 3$.

3.1 Analysis Strategy and Performance Metrics

DT track segments, built by the local offline reconstruction software independently within each chamber crossed by an incoming muon, are used as proxy to evaluate the DT local trigger performance. The track segment reconstruction in the barrel DT chambers [2] proceeds as follows: i) a hit reconstruction consisting in deriving spatial points from the time measurements in each DT cell occurs; ii) a combinatorial pattern recognition is

used to identify and group all the hits belonging to the same track; iii) a linear fit of these points is performed. Until this point, track segments are built independently in the ϕ-SLs and θ-SLs of a DT chamber, and they are combined only at the latest stage of the DT local reconstruction. Together with the position and the direction of a track segment, the linear fit also measures the crossing time (t_0) of an incoming particle. Such t_0 is calibrated so that it is, on average, 0 for prompt muons of infinite energy that traverse a given chamber.

The reconstructed track segments are matched with the generated muons by selecting the ones that:

- are built using at least 4 hits from the two ϕ-SLs of a chamber;
- the difference in radial coordinates between the generated muon direction and the segment position is: $\Delta\phi < 0.2$;
- the difference in longitudinal coordinates between the generated muon direction and the segment position is: $\Delta\eta < 0.15$ if the segment has a component in the θ-SL, $\Delta\eta < 0.30$ otherwise;
- have a $|t_0| < 15$ ns;

If multiple segments per station satisfy all the above criteria, the one that is reconstructed using more hits from the ϕ-SLs is selected. Out of this selection, each muon can be matched to, at most, four segments, one for each of the DT stations from MB1 to MB4.

All DT local trigger algorithms operate within a single chamber and they are able to produce preliminary track segments, called trigger primitives, that contain the information of the chamber in which they have been built (station, wheel and sector), as well as additional quantities such as their BX of origin, their position, direction and a quality flag.

Position and direction are provided for each trigger primitive by means of the ϕ and ϕ_B coordinates presented in Fig. 3.1. The ϕ coordinate is the radial position of a trigger primitive, computed with respect to an axis defined, for each sector, as the line perpendicular to the chamber that intersects the CMS interaction point. The ϕ_B is defined as the difference between ϕ and the segment local direction ψ. It represents the additional bending that a curved muon, coming from the interaction point, has with respect to a straight line trajectory. Out of ϕ, the local x coordinate, representing the position in cm of a segment with respect to the center of a chamber, is computed and used in the following.

DT trigger primitives include a quality flag, which represents the number of hits used to build a given primitive and their position within the two ϕ-SLs of a chamber, as explained in chapter 2.

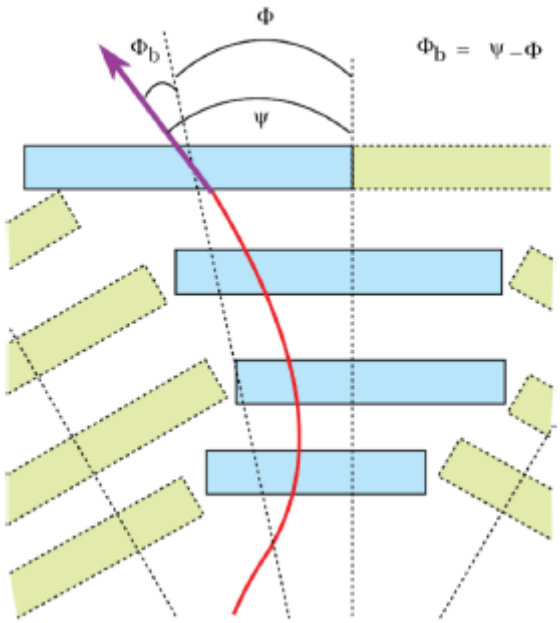

Figure 3.1: Trigger Primitives angular parameters definition.

Throughout the rest of the analysis, only trigger primitives which are geometrically close to track segments matched with generated muons are considered. The matching between trigger primitives and track segment is performed by considering all triggers that:

- are in the same station, wheel and sector of the segment;
- are less than 5 cm apart from the segment in the local x coordinate.

All triggers matched to a segment according to the logic described above are considered for the study. Out of them, a "reference trigger" is looked for by selecting the primitive with the highest quality, among the ones which correctly identify the BX of origin of the generated muon.

The trigger efficiency, computed with respect to reconstructed track segments, is hence defined as the fraction of segments for which is possible to identify a reference trigger. It is measured independently for each MB station.

Trigger efficiencies for different algorithms computed as function of the generated muon eta and p_T are shown, respectively, in Fig. 3.2 and Fig. 3.3. In both figures, AM and HB algorithms efficiencies are shown to be slightly higher ($\sim$ 98%) than the one of the Phase-1 algorithm ($\sim$ 96%). In the plot versus η, the efficiency drops in correspondence of cracks between wheels. In the plot versus p_T, the efficiency shows only a very mild dependence on the transverse momentum.

The local trigger reconstruction is based on the processing of multiple groups of cells (e.g. a BTI) which partly overlap with each other. Additionally, due to combinatorics of hits involved in the pattern recognition, spurious hits alignments forming an approximate straight line track are possible. Therefore, in a fraction of cases, more than one trigger primitive is generated within a given chamber and for a single crossing muon. Those multiple copies of trigger primitives are usually referred as "ghosts". In this analysis, we define ghosts as all trigger primitives that are matched with a reconstructed segment beyond the reference trigger. The fraction of events with ghosts is found by dividing the number of events with more than one trigger primitive by the number of events characterized by the presence of a reference trigger. Two different definitions of ghosts are used. The first (Fig. 3.4 and 3.5) is obtained by selecting only the trigger primitives in time with the collision, by excluding all triggers with a different BX. The second one is done without this selection (Fig. 3.6 and 3.7). In the rest of the text, we refer to those two definitions as "in time" ghosts and ghosts at "any BX" respectively.

The ghost fraction from the HB method is significantly higher than the ghost fraction from both the AM and Phase-1 trigger algorithms. This conclusion holds for all stations. In particular, the fraction of triggers with in time ghosts for HB is around 13%, while AM and Phase-1 are around 3% and 1% respectively. Similar conclusions hold for the fraction of ghosts at any BX, which for HB is slightly less than 20%, while AM and Phase-1 are both between 6% and 8%, with the AM generating, in MB1/2/3 stations, roughly 1% less ghosts than the Phase-1 algorithm.

3.2 Stability of the Analysis in Samples with Pile-Up

The results presented until now were obtained using samples that included no simulation of overlapping pile-up collisions on top of the pair of back to back muons generated flat in ϕ, η and p_T. However, at the peak luminosity expected for HL-LHC one expects, on average, $\sim$ 200 collisions for each bunch crossing. Therefore, the analysis presented in the previous section was repeated using a simulated sample which included a mean pile-up of 200 collisions per event overlayed on top of the signal muons used for the study. A comparison is performed, between results obtained from samples with and without pile-up, for all algorithms in terms of efficiency and fraction of events with ghosts (both in time and at any BX). Plots (Fig.s 3.8, 3.9) show no significant difference.

These results indicate that, given the low hit occupancy expected for the barrel region of the muon spectrometer, pile-up has a negligible impact on the performance figures used for this study. Therefore, in the rest of the chapter, we will keep using the sample with no overlapping pile-up collisions, as the interpretation of the mechanisms generating ghost triggers is more straightforward if such sample is used.

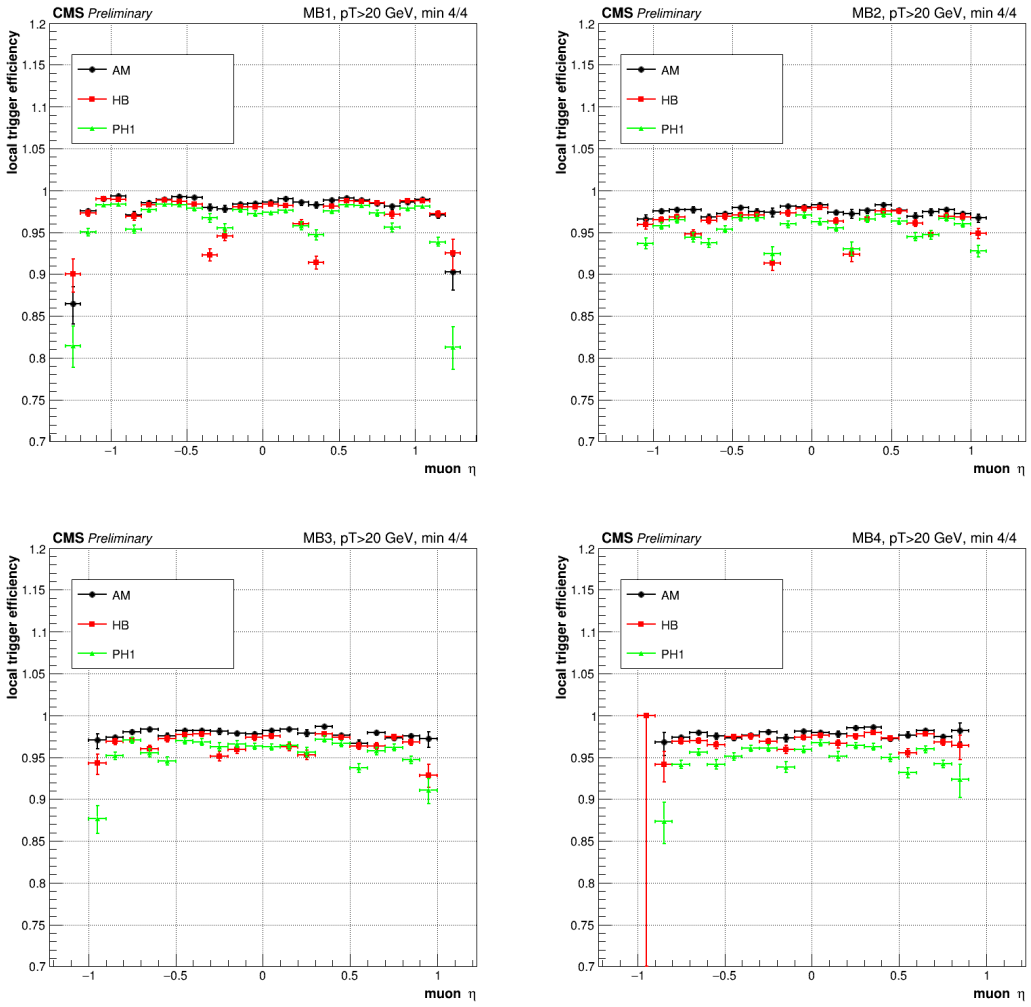

Figure 3.2: Efficiency as function of the pseudorapidity of generated muons for all the stations (top left: MB1; top right: MB2; bottom left: MB3; bottom right: MB4). Black and red points are computed respectively for the AM and HB Phase-2 algorithms. Green points are computed for the Phase-1 algorithm.

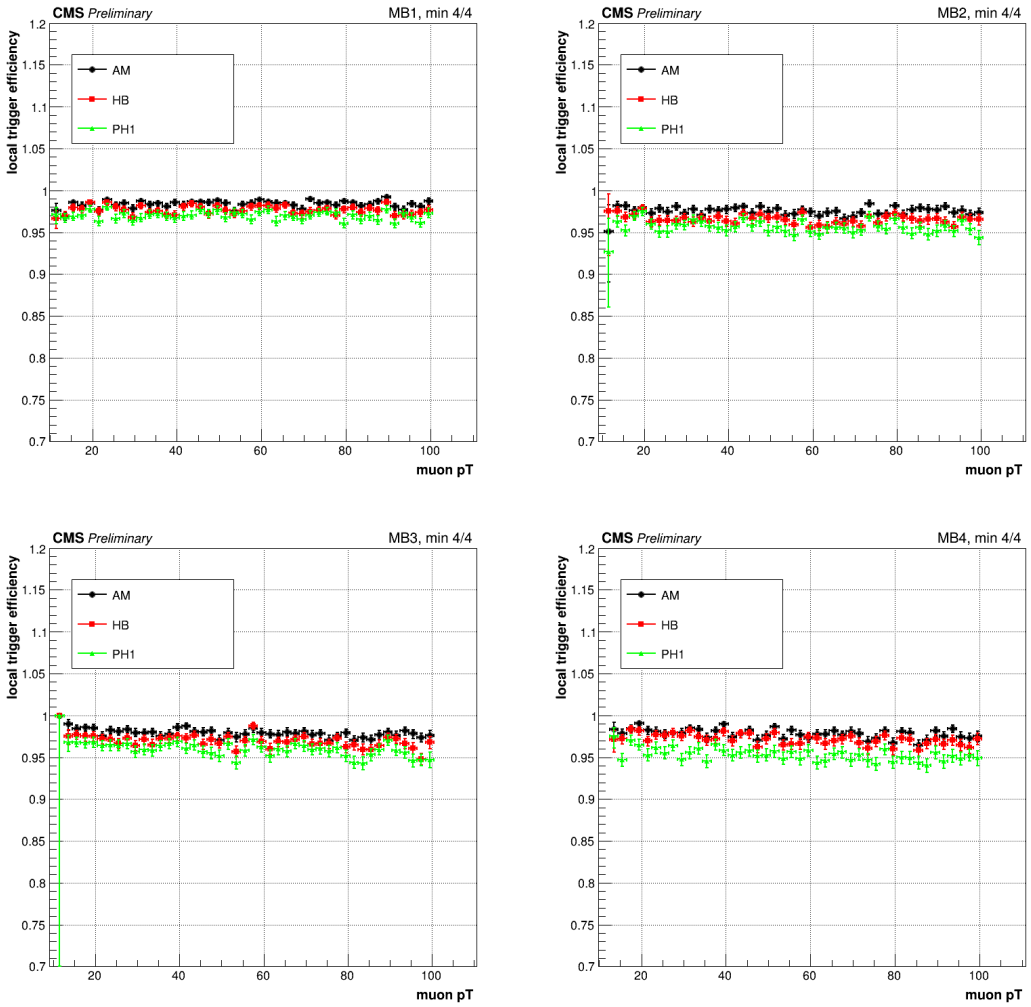

Figure 3.3: Efficiency as function of the transverse momentum of generated muons for all the stations (top left: MB1; top right: MB2; bottom left: MB3; bottom right: MB4). Black and red points are computed respectively for the AM and HB Phase-2 algorithms. Green points are computed with the Phase-1 algorithm.

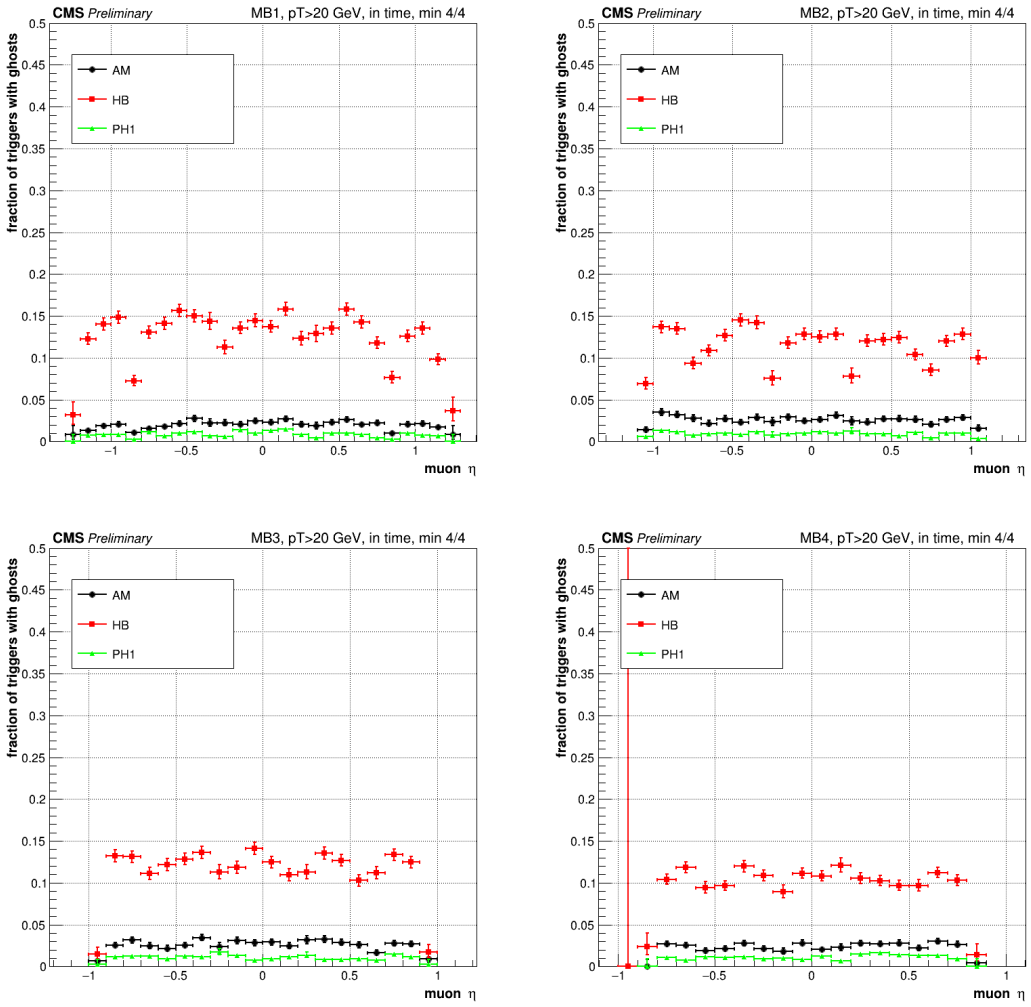

Figure 3.4: Fraction of triggers with in-time ghosts as function of the pseudorapidity of generated muons for all the stations (top left: MB1; top right: MB2; bottom left: MB3; bottom right: MB4). Black and red points are computed respectively for the AM and HB Phase-2 algorithms. Green points are computed with the Phase-1 algorithm.

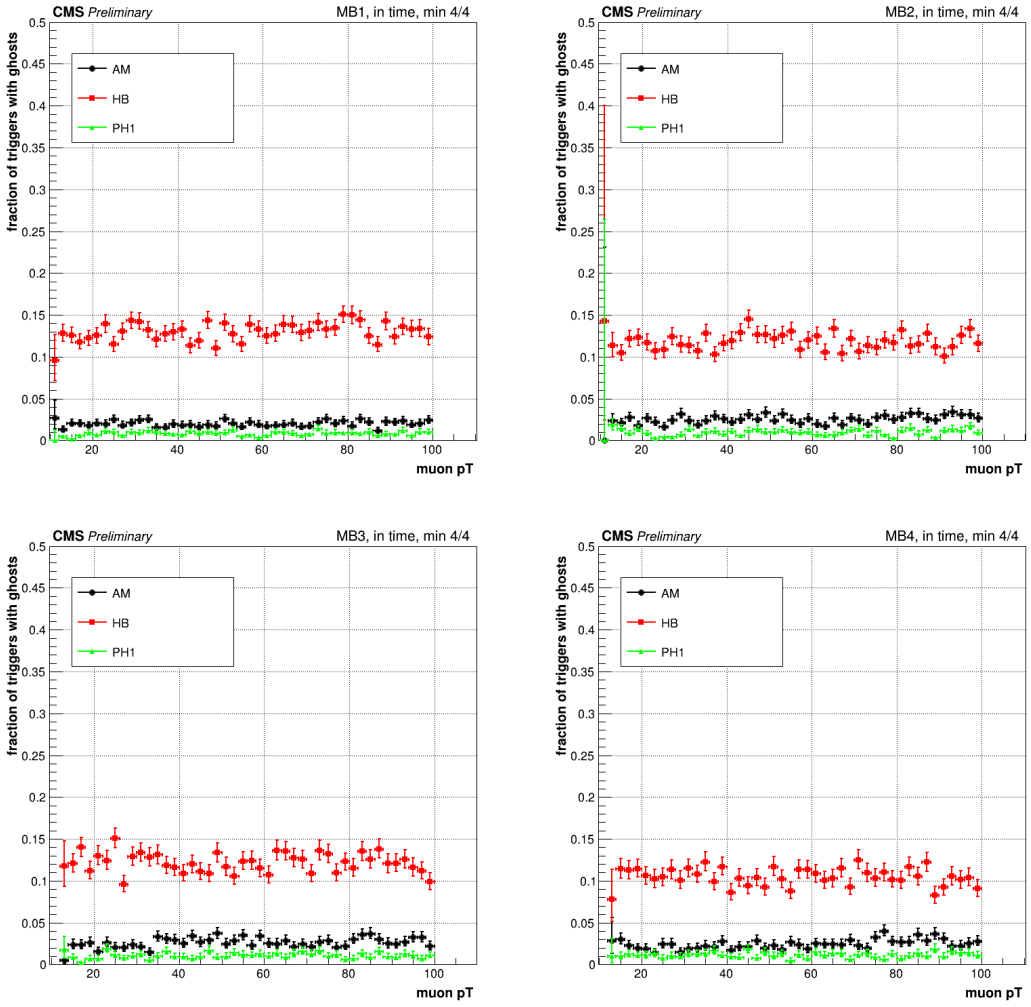

Figure 3.5: Fraction of triggers with in-time with ghosts as function of the transverse momentum of generated muons for all the stations (top left: MB1; top right: MB2; bottom left: MB3; bottom right: MB4). Black and red points are computed respectively for the AM and HB Phase-2 algorithms. Green points are computed with the Phase-1 algorithm.

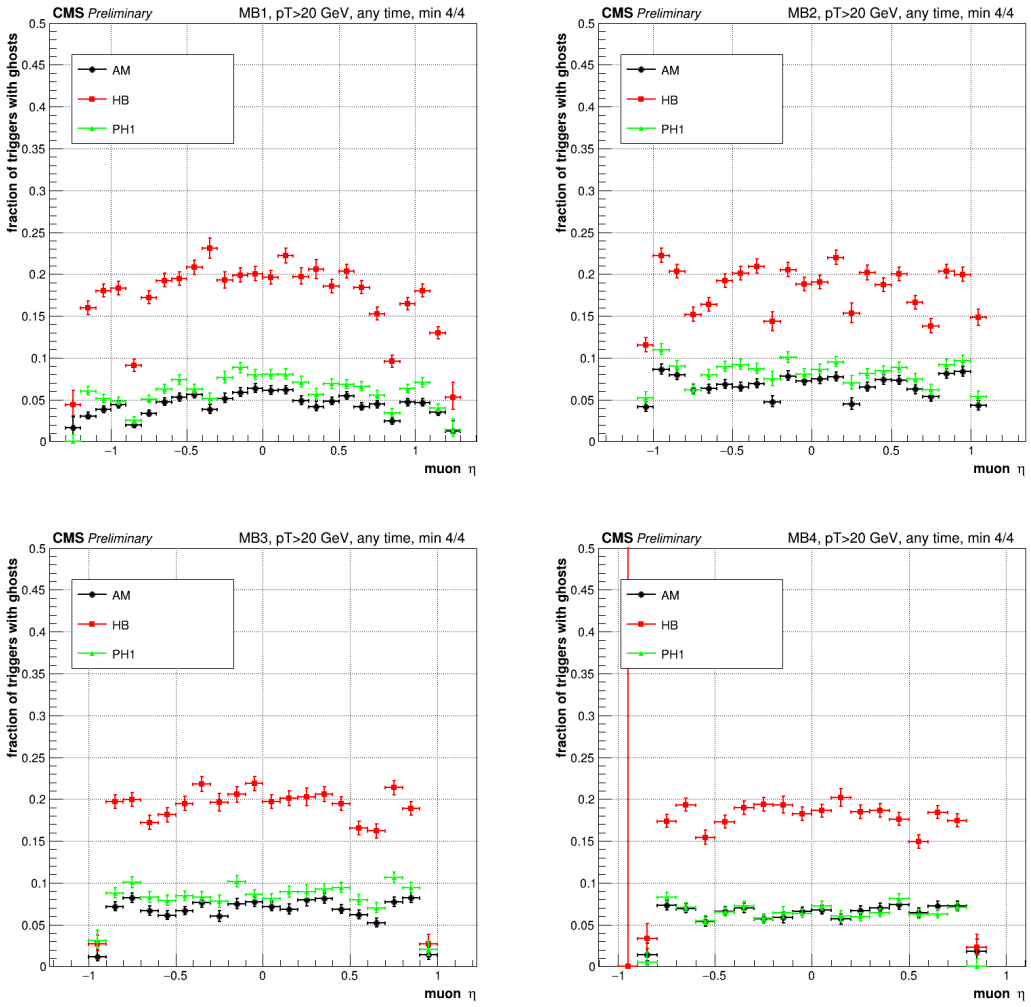

Figure 3.6: Fraction of triggers with ghosts at any BX as function of the pseudorapidity of generated muons for all the stations (top left: MB1; top right: MB2; bottom left: MB3; bottom right: MB4). Black and red points are computed respectively for the AM and HB Phase-2 algorithms. Green points are computed with the Phase-1 algorithm.

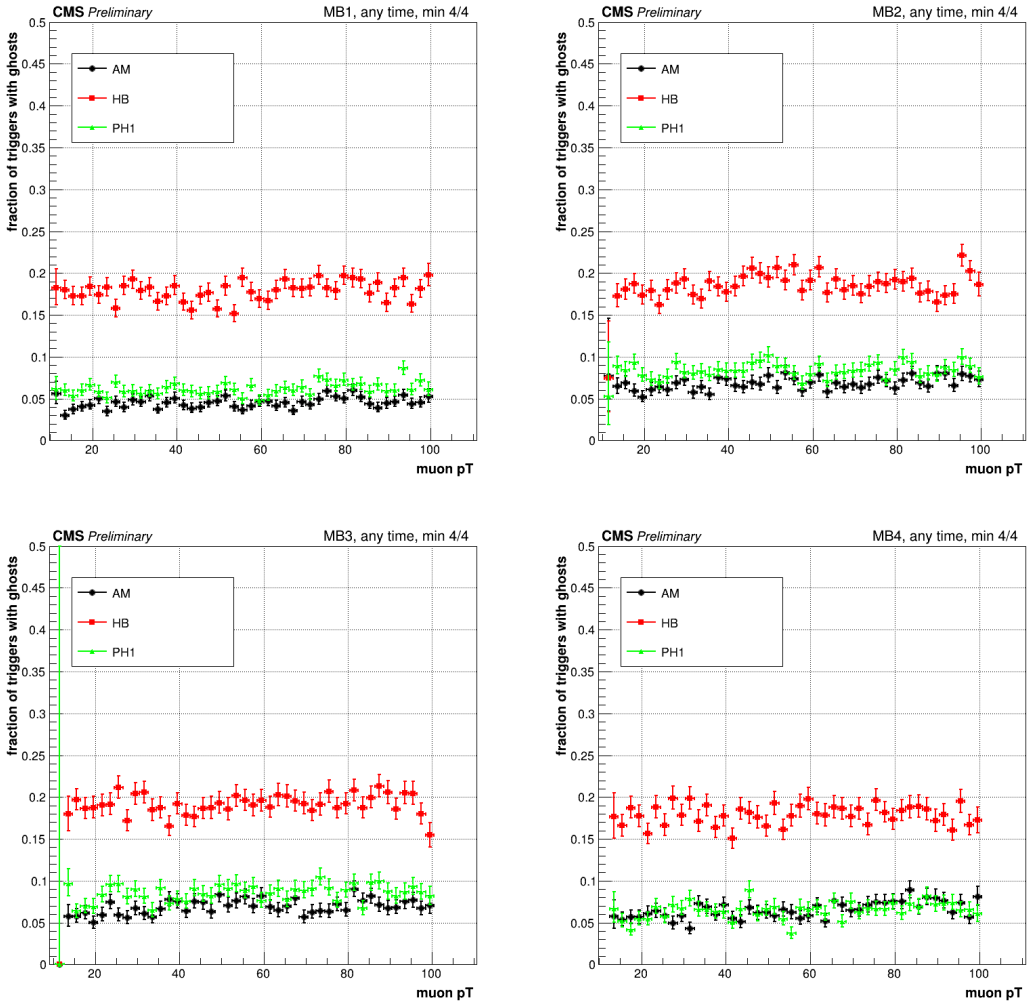

Figure 3.7: Fraction of triggers with ghosts at any BX as function of the transverse momentum of generated muons for all the stations (top left: MB1; top right: MB2; bottom left: MB3; bottom right: MB4). Black and red points are computed respectively for the AM and HB Phase-2 algorithms. Green points are computed with the Phase-1 algorithm.

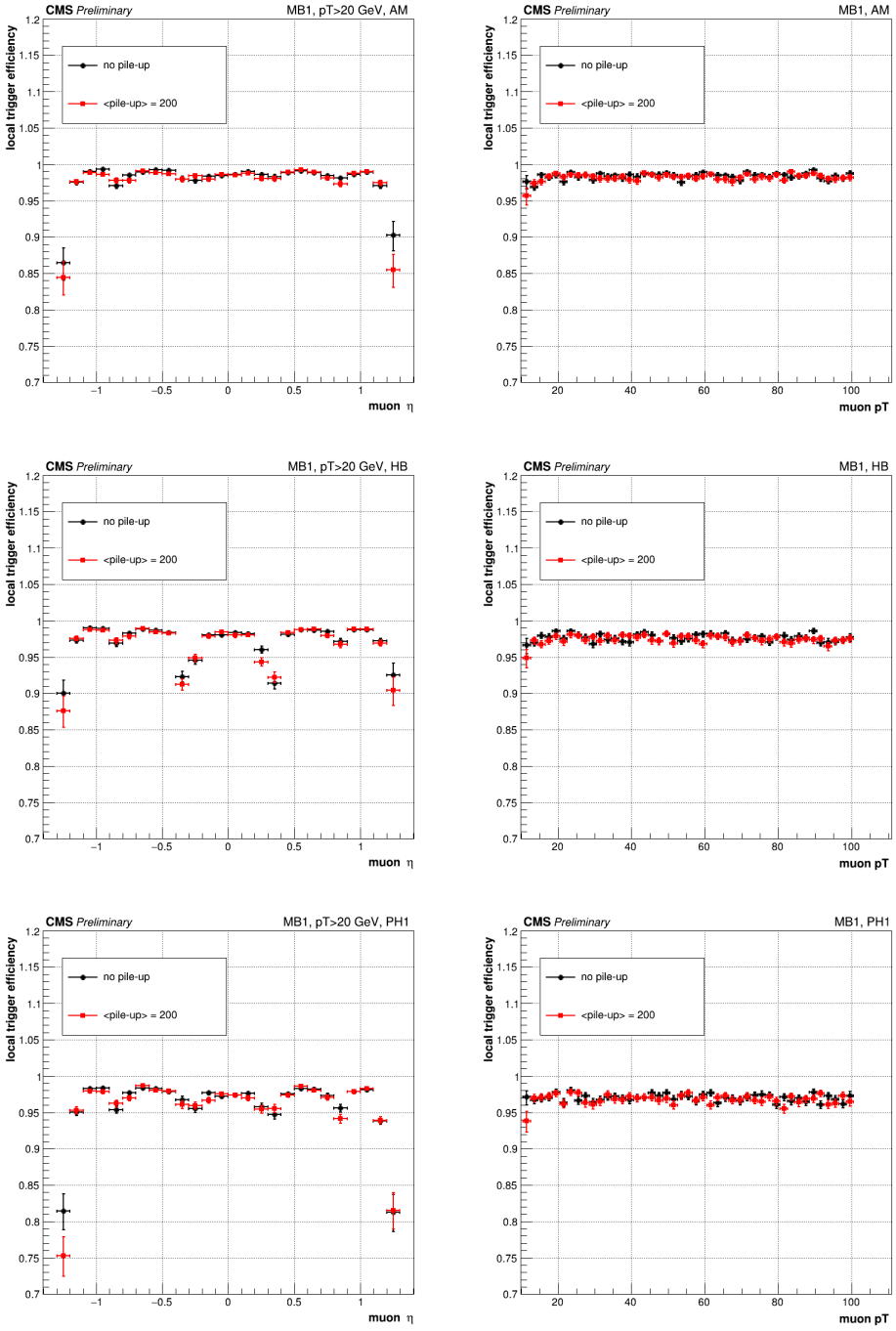

Figure 3.8: Efficiency as function of the pseudorapidity of generated muons (left) and as function of the transverse momentum of generated muons (right) for all algorithms (from top to bottom: AM, HB, Phase-1). Black and red points refer to ghosts at any-BX, computed respectively without and with pile-up. All efficiencies refer only to the MB1 station.

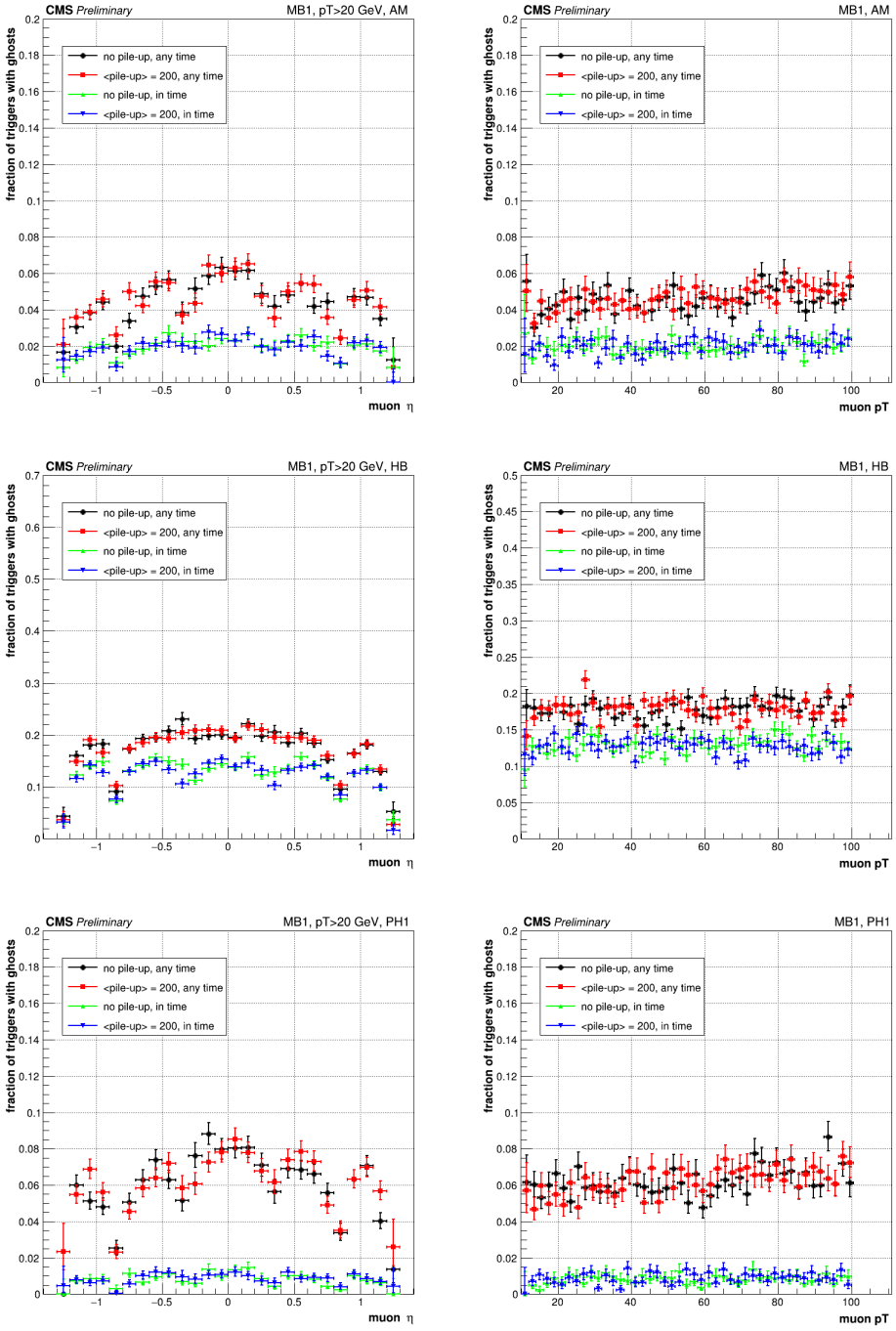

Figure 3.9: Fraction of triggers with ghosts as function of the pseudorapidity of generated muons (left) and as function of the transverse momentum of generated muons (right) for all algorithms (from top to bottom: AM, HB, Phase-1). Black and red points refer to ghosts at any-BX, computed respectively without and with pile-up. Similarly, green and blue points refer to in-time ghosts. All ghost fractions refer only to the MB1 station.

3.3 Study of different Quality Categorizations

One way to reduce the fraction of triggers with ghosts would be to only accept trigger primitives with a higher quality. Of course, if less ghosts are produced, the efficiency might also decrease because low quality triggers get rejected. Therefore, it is interesting to check if an optimal trade-off between these two figures can be identified.

For this reason, trigger efficiency and ghost fractions are studied with five different set of qualities. Details on the the definition and the naming of these different sets are in Table 3.1.

Phase-1 qualities	**AM qualities**	**HB qualities**	**Code name**
/	all qualities	all qualities	Min 3/4
/	3,4,5,6,7,8,9	4,5,6,7,8,9	Min 3/4 +2
2,3,4,5,6	3,4,6,7,8,9	4,6,7,8,9	Min 4/4
/	6,7,8,9	6,7,8,9	Min 4/4 +2
4,5,6	6,8,9	6,8,9	Correlated

Table 3.1: Definition and naming of different quality sets for each algorithm (AM, HB and Phase-1). Quality numbers refer to the ones described in Table 2.1

In general, raising the acceptable qualities of the trigger primitives lowers both efficiency and fraction of ghosts. This behavior is consistent among all algorithms. In fact, with different quality sets, efficiency for both AM (Fig. 3.10) and HB (Fig. 3.11) spans between 98% and 88%. In a similar way, for AM the fraction of in time ghosts goes from 4% to 1%, while for HB it drops from 14% to 2%. The fraction of events with ghosts at any BX for AM spans from 8% to 1%, while for HB it goes from 30% to 7%.

The next step is understanding which sets of quality cuts leads to optimal performance, meaning the one that compromises between the highest efficiency and the lowest fraction of ghosts possible.

The results of this study are shown in Fig. 3.16 and Fig. 3.17, where efficiencies for different quality sets are plotted versus the respective fraction of in time ghosts and ghosts at any BX. In Fig. 3.16 each point is color coded according to the quality cut. From this figure, the optimal set of qualities appears to be Min 4/4. This is actually true for all algorithms and when considering both in time ghosts and ghosts at any BX.

Figure 3.17 shows that, for AM, Min 4/4 has a 98.5% efficiency with a fraction of ghosts of 2% (in time) or 4.5% (any BX). For HB, Min 4/4 is found to be 98% efficient with a ghost fraction of 15% (in time) or 20% (any BX). For Phase-1, Min 4/4 has a 97% efficiency with a fraction of ghosts of 1% (in time) or 6% (any BX).

Min 4/4 +2 shows an increase in the fraction of ghosts, both for AM and HB, which requires further explanation. This discrepancy is due to the significant drop in efficiency

compared with Min 4/4: since the fraction of events with reference triggers is significantly lower, the ghost fraction rises, even if the number of ghosts is roughly unchanged.

Finally, a study which compares the quality of the reference trigger with the ones of ghost triggers is performed. The objective of this test is to identify the "types" of triggers which are more prone to generate ghosts, as well as the relation between the two, with the hope that this can help improving the ghost rejection mechanisms of the Phase-2 algorithms. As expected, no in time ghosts are found with an higher quality than the one of the best trigger. For AM (Fig. 3.18 - left), the most common mechanism that produces in time ghosts generates a reference trigger of quality 4+2, with a ghost quality of 3+2. For HB (Fig. 3.19 - left), the most common reference trigger have a quality of 4+4, with ghost qualities of 4+2 and 4/4. For the Phase-1 algorithm (Fig. 3.20 - left), both the most common reference trigger and ghost quality is 4+3.

All algorithms have a low number of ghosts at any BX with a higher quality than the reference trigger. For AM (Fig. 3.18 - right), more ghosts are found when the reference trigger has a quality of 4+2 and 3+2, with respectively the same ghost quality. For HB (Fig. 3.19 - right), ghosts can have a pretty varied quality if the reference trigger quality is higher than 4+2. In particolar, many ghosts with quality 3+2 are found if the trigger quality is 4+3. For the Phase-1 algorithm (Fig. 3.20 - right), many more ghosts are found with the same qualities as the reference trigger ones (4/4 and 3+3 in particular), as well as ghosts with quality 3+3 or lower when the quality of the reference trigger is 4+3 or 4+4. The Phase-1 algorithm also finds many 4/4 ghost triggers when the reference trigger also has 4/4 quality because the TRACO correlates only BTI trigger segments which are reconstructed at the same BX. In case one of the BTIs from the two DT ϕ-SL wrongly assigns the trigger BX no correlation is attempted, hence ghosts with a quality pattern as the one observed in the figure are generated.

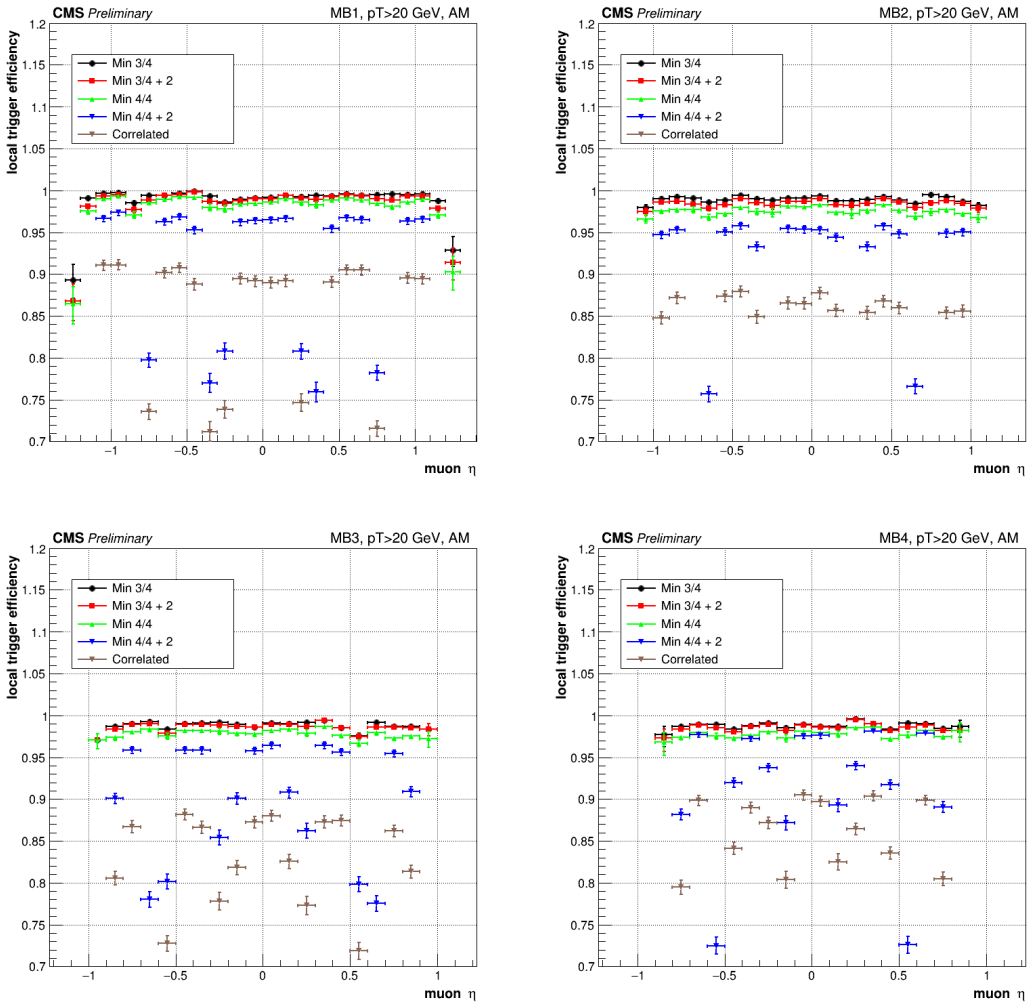

Figure 3.10: Efficiency as function of the pseudorapidity of generated muons for the AM Phase-2 algorithm for all the stations (top left: MB1; top right: MB2; bottom left: MB3; bottom right: MB4). Different colors refer to different combinations of qualities, as described in Tab. 2.1

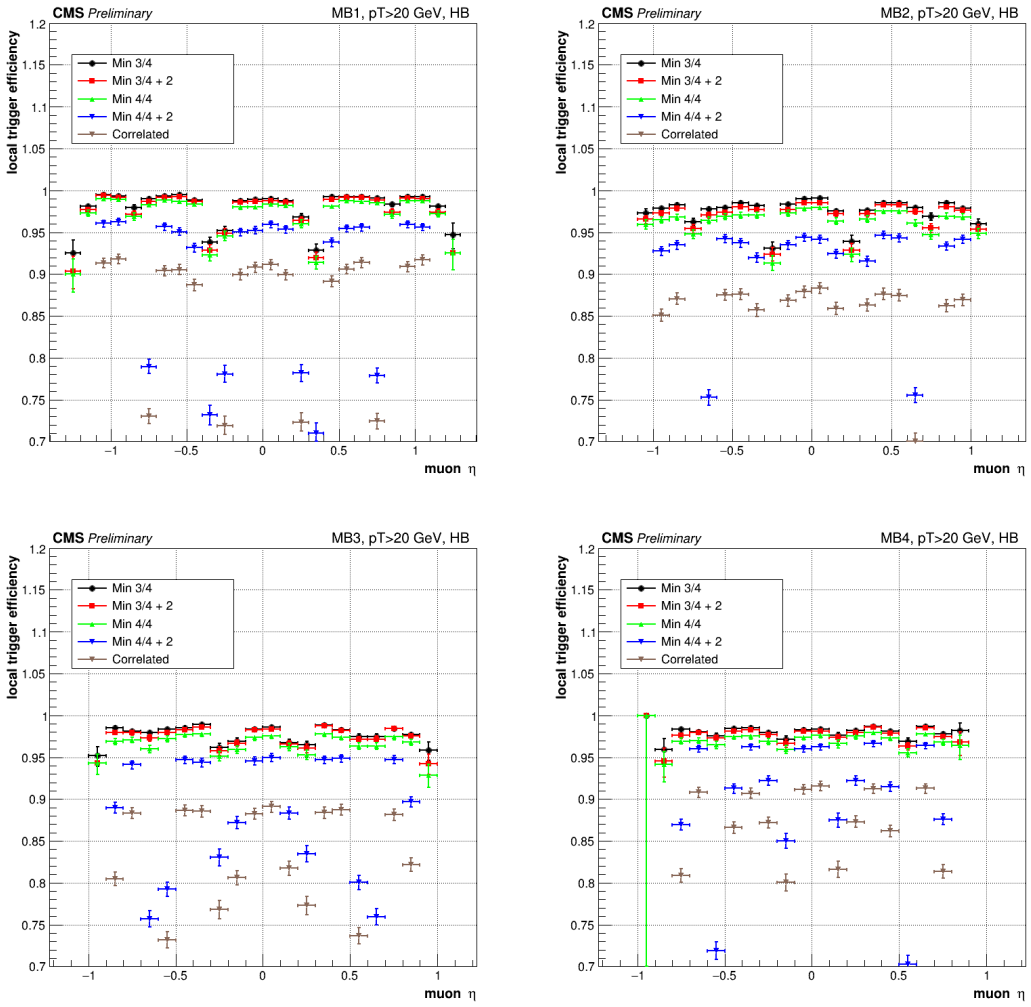

Figure 3.11: Efficiency as function of the pseudorapidity of generated muons for the HB algorithm for all the stations (top left: MB1; top right: MB2; bottom left: MB3; bottom right: MB4). Different colors refer to different combinations of qualities, as described in Tab. 2.1

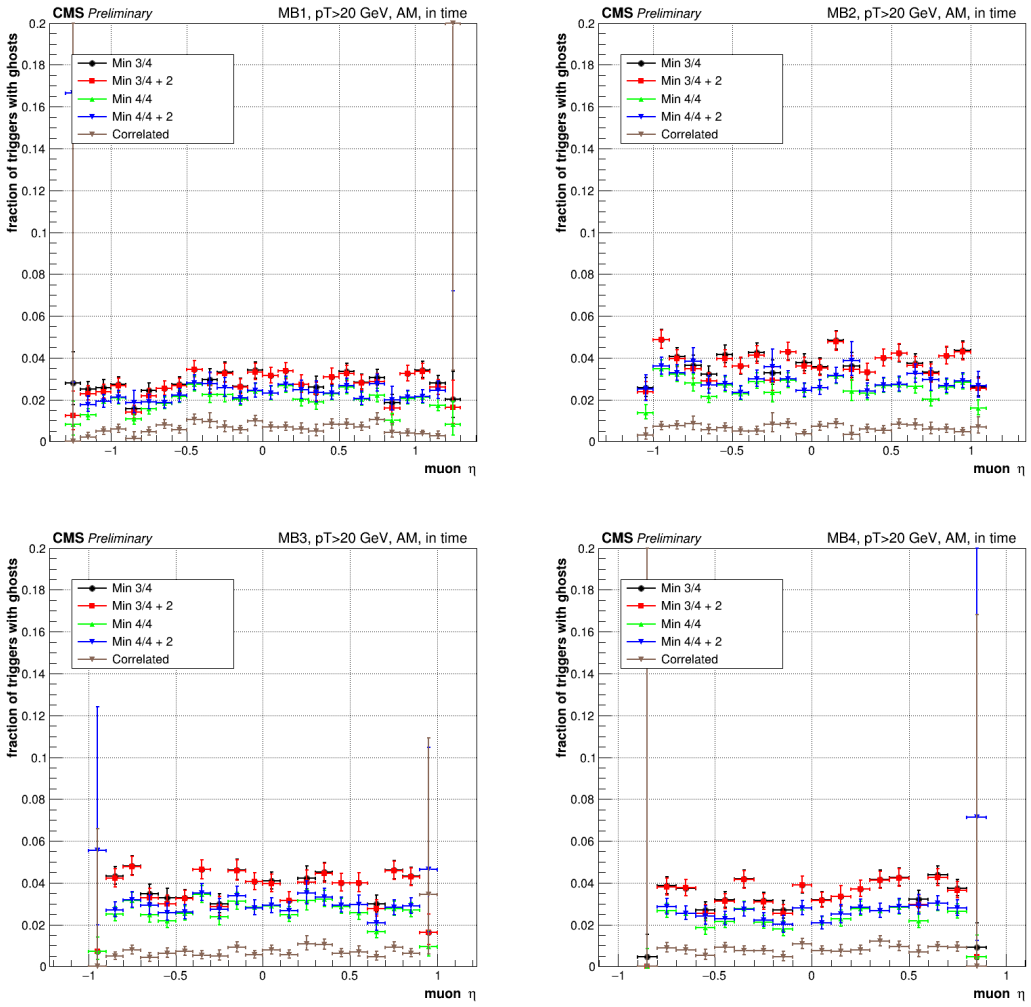

Figure 3.12: Fraction of trigger with in-time ghosts as function of the pseudorapidity of generated muons for the AM algorithm for all the stations (top left: MB1; top right: MB2; bottom left: MB3; bottom right: MB4). Different colors refer to different combinations of qualities, as described in Tab. 2.1.

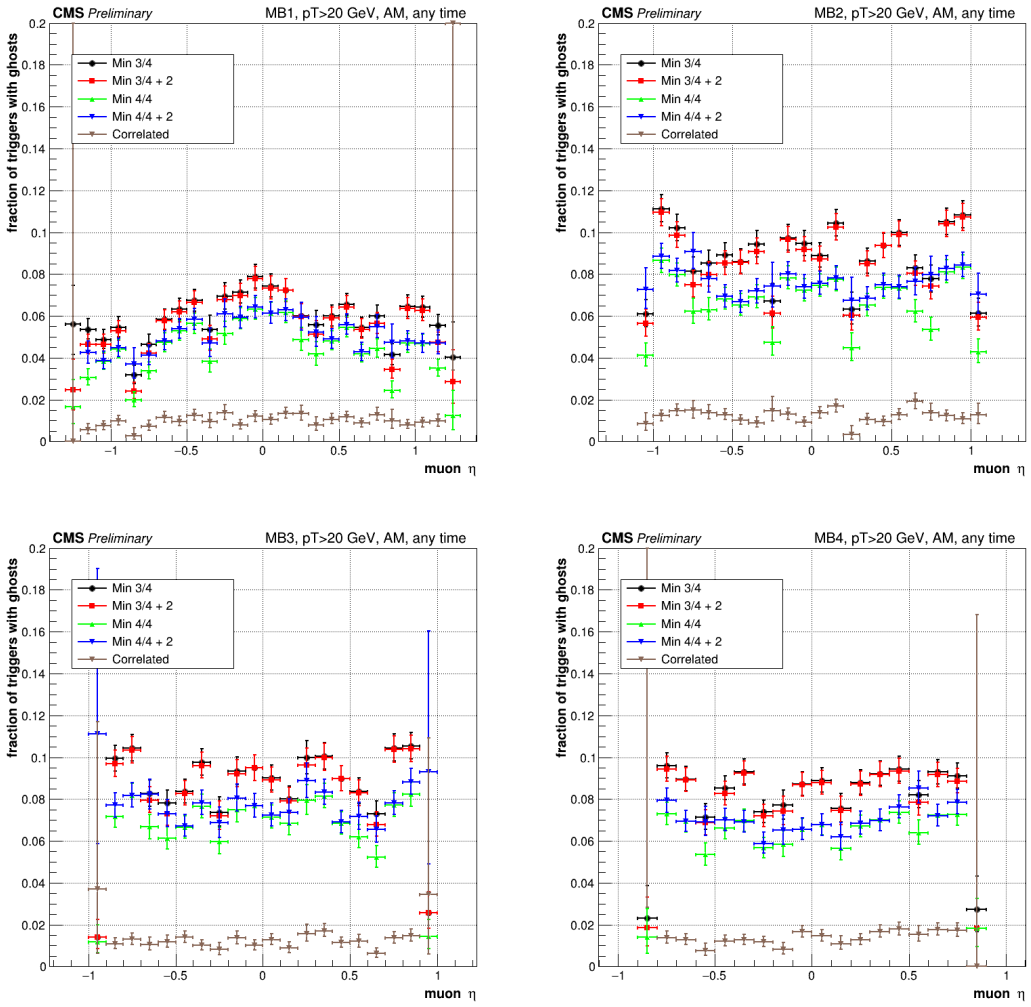

Figure 3.13: Fraction of trigger with ghosts at any BX as function of the pseudorapidity of generated muons for the AM algorithm for all the stations (top left: MB1; top right: MB2; bottom left: MB3; bottom right: MB4). Different colors refer to different combinations of qualities, as described in Tab. 2.1.

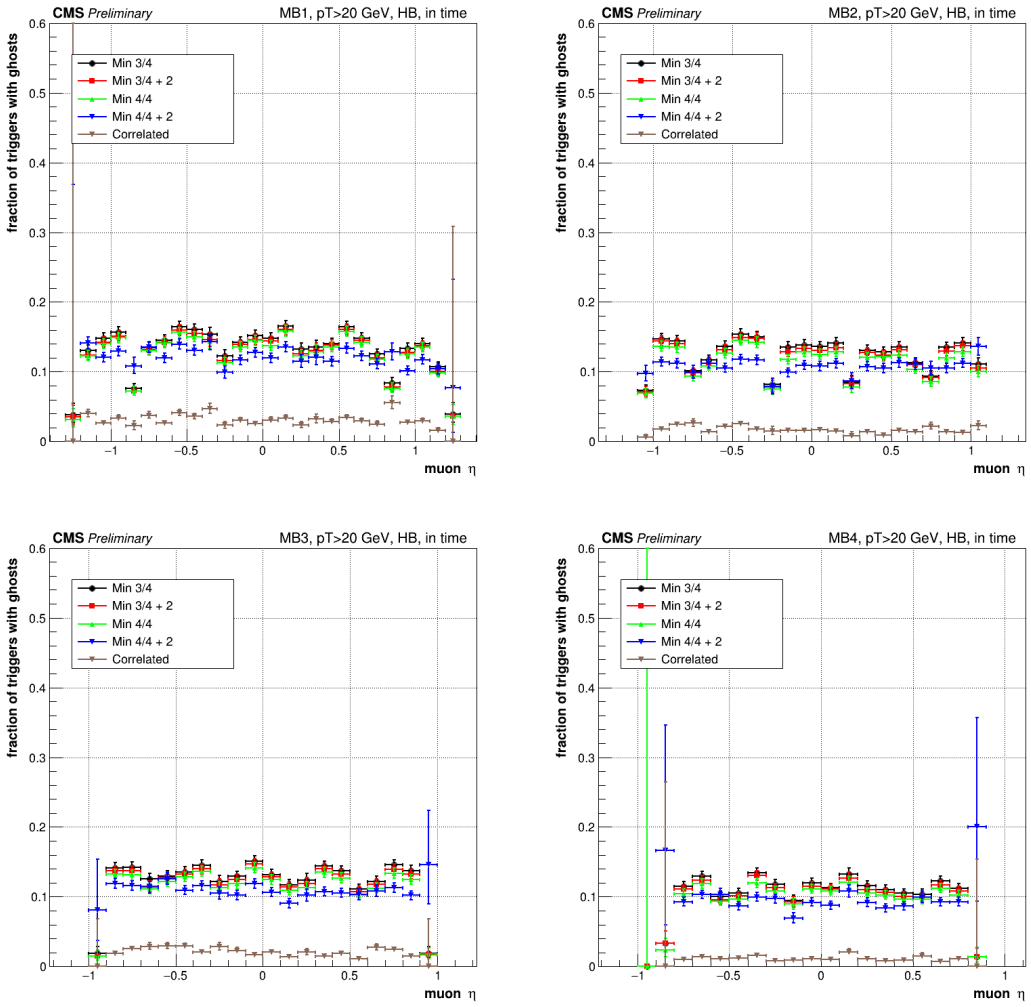

Figure 3.14: Fraction of trigger with in-time ghosts as function of the pseudorapidity of generated muons for the HB algorithm for all the stations (top left: MB1; top right: MB2; bottom left: MB3; bottom right: MB4). Different colors refer to different combinations of qualities, as described in Tab. 2.1.

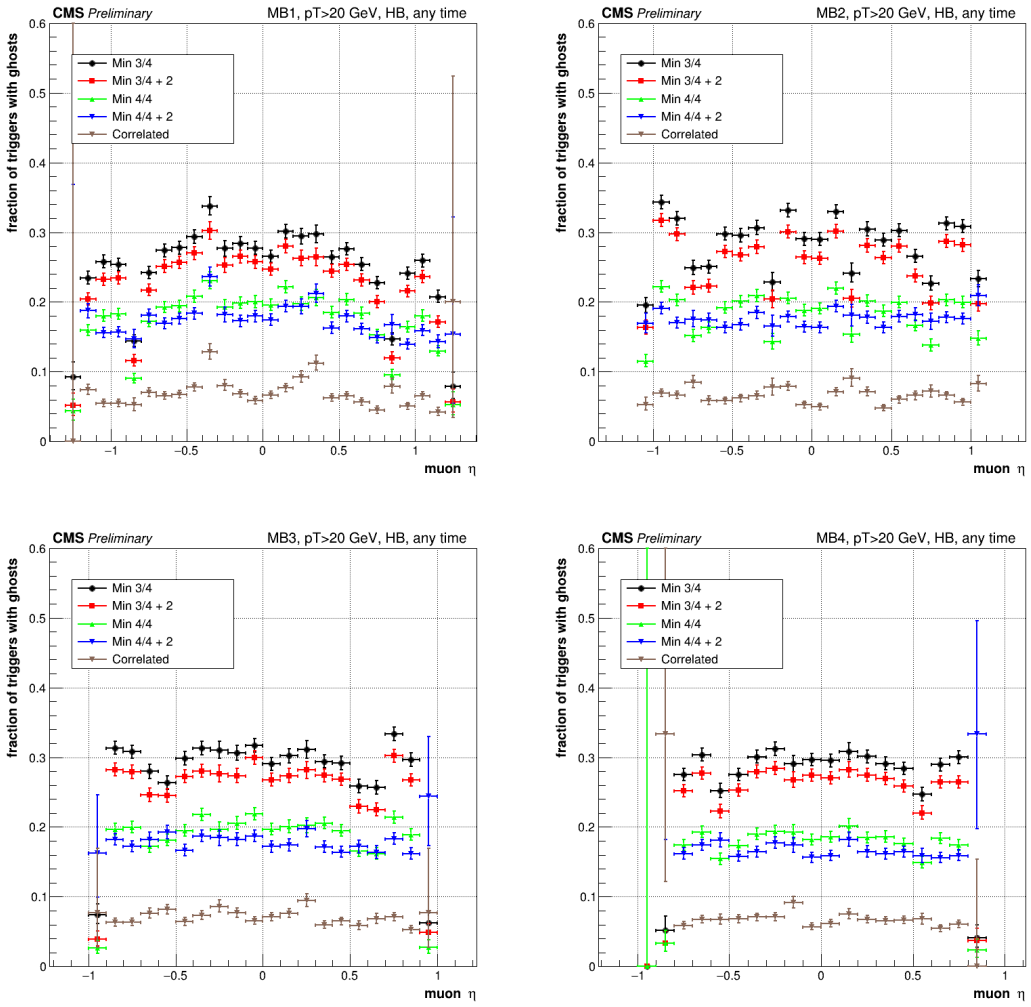

Figure 3.15: Fraction of trigger with ghosts at any BX as function of the pseudorapidity of generated muons for the HB algorithm for all the stations (top left: MB1; top right: MB2; bottom left: MB3; bottom right: MB4). Different colors refer to different combinations of qualities, as described in Tab. 2.1.

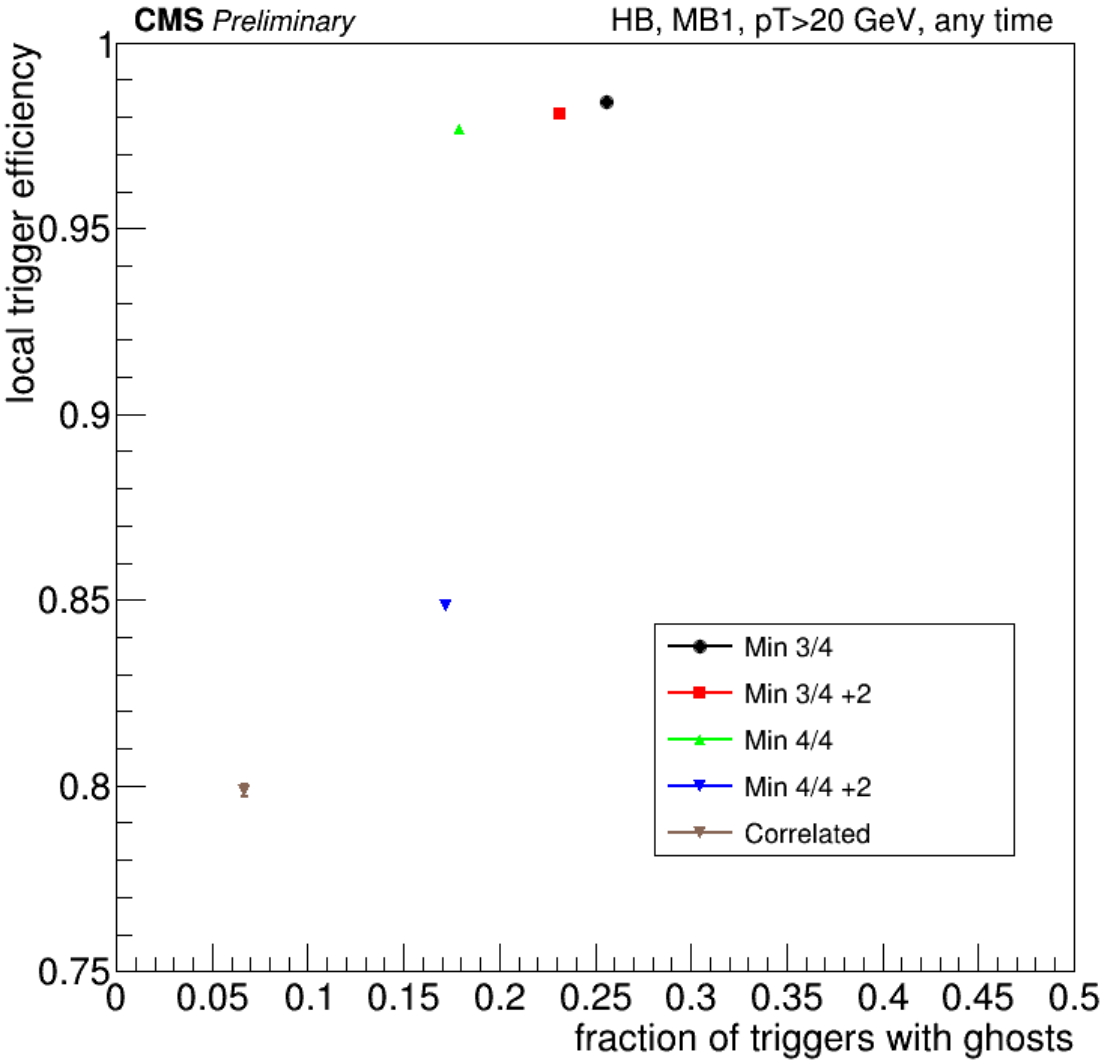

Figure 3.16: Trigger efficiency versus fraction of events with ghosts for the HB algorithm. Different colors refer to different combinations of qualities, as described in Tab. 2.1. Results are reported for the MB1 station.

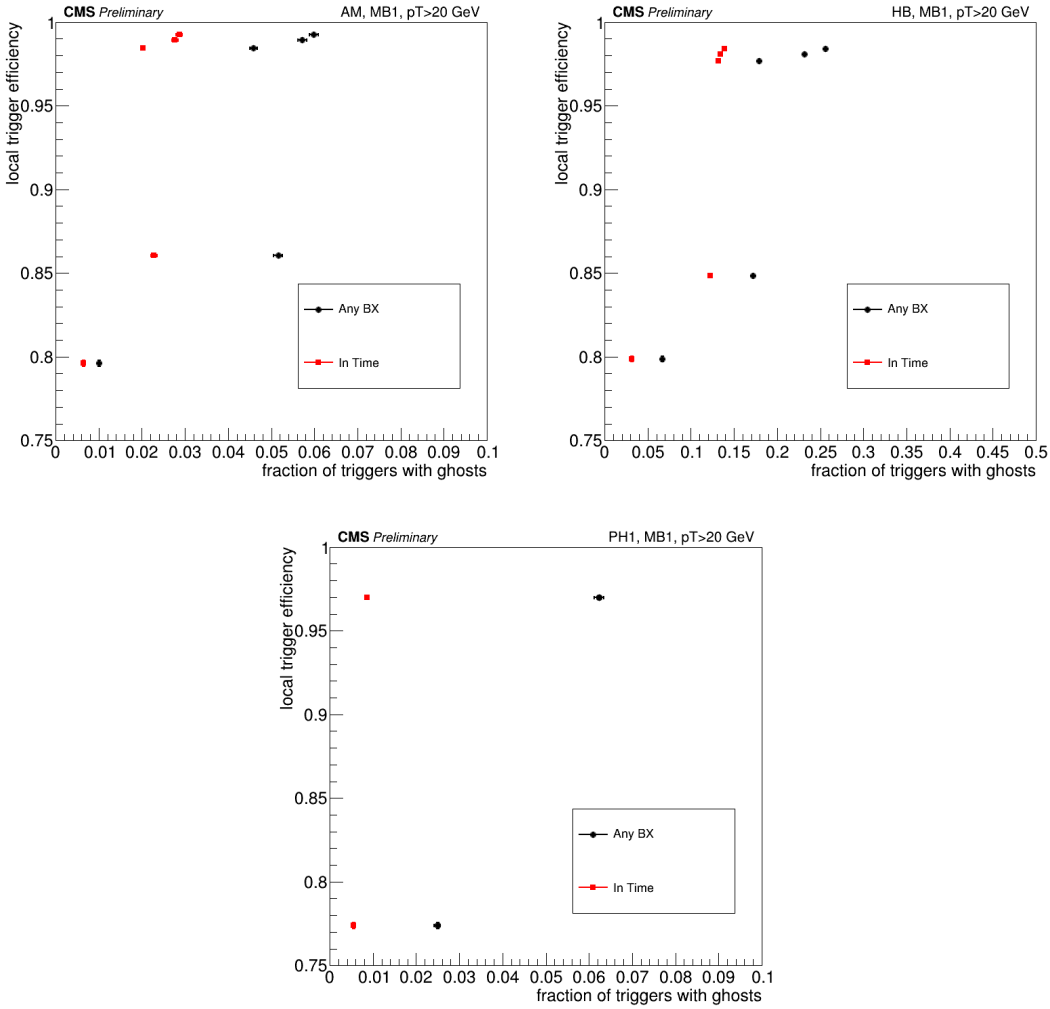

Figure 3.17: Trigger efficiency versus fraction of events with ghosts for all algorithms (top left: AM, top right: HB, bottom: PH1). Red points and black point are computed respectively with and without time restriction. Results are reported for the MB1 station.

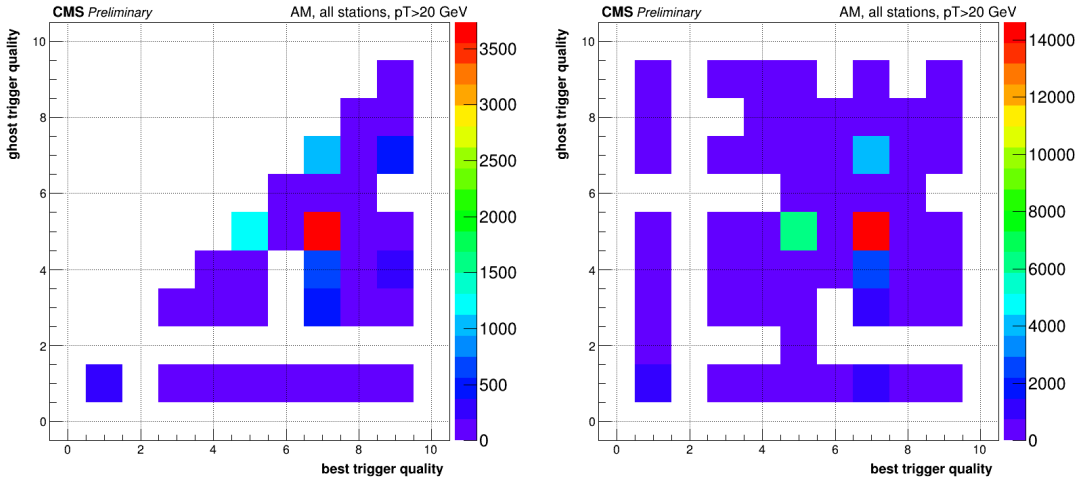

Figure 3.18: Ghost trigger quality versus best trigger quality for the AM algorithm for different time restrictions. Results are computed for in-time ghosts (left) and ghosts at any BX (right).

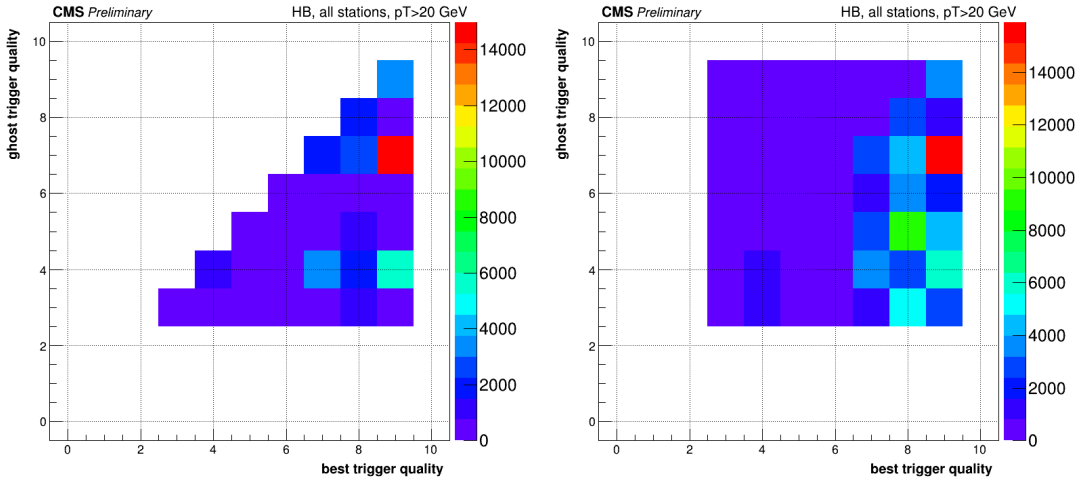

Figure 3.19: Ghost trigger quality versus best trigger quality for the HB algorithm for different time restrictions. Results are computed for in-time ghosts (left) and ghosts at any BX (right).

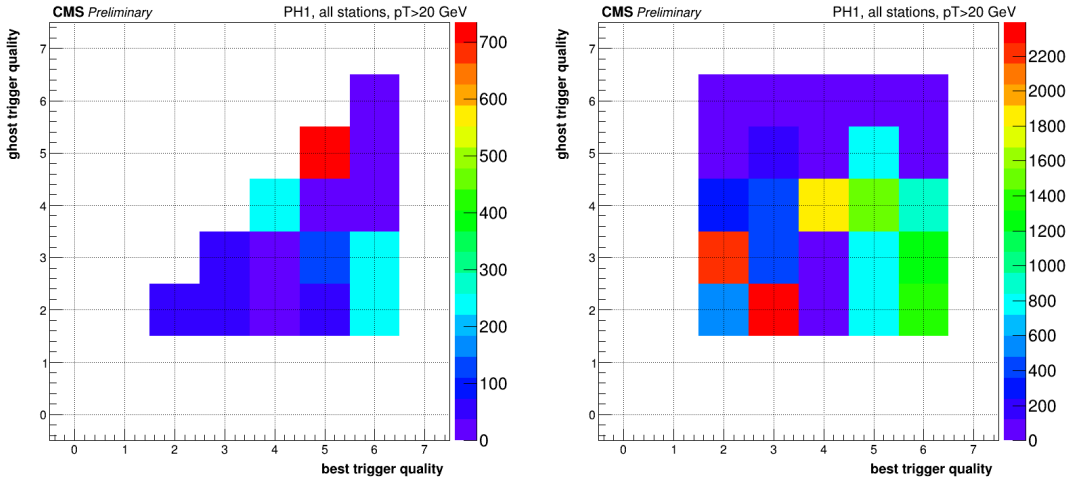

Figure 3.20: Ghost trigger quality versus best trigger quality for the Phase-1 algorithm for different time restrictions. Results are computed for in-time ghosts (left) and ghosts at any BX (right).

Conclusions

In this thesis, the performance of two CMS Drift Tubes local trigger algorithms proposed for HL-LHC is studied. The proposed algorithms are called Analytical Method (AM) and Histogram-Based (HB) and their performance is studied in comparison to the algorithm currently in use. An analysis tool has been developed to study samples of simulated data by measuring the trigger performance in events with segments reconstructed offline. Two figures related to the performance of the trigger were studied: the efficiency and the fraction of cases in which more than a trigger segment is produced by a single muon traversing a chamber (ghost). Ghosts have been evaluated both considering those produced in-time with the muons traversing the detector, as well as the ones that got wrongly assigned a different time. These figures are computed as a function of the muon transverse momentum and pseudorapidity independently in each station, to test the uniformity of the performance in all the detector within the probed energy range. In addition, the metrics described above have been measured for different categories of a quality variable representing the number of hits used to reconstruct a trigger segment. The goal was to identify the quality set with higher performance, meaning the one with the best trade-off between efficiency and fraction of ghosts.

The results presented in this thesis show that, for equivalent quality categorizations, the local trigger efficiency from the proposed algorithms are approximately 1% higher than the ones from the present algorithm. The fraction of ghost from the AM and the present trigger have been found to be consistent. However, the one from HB algorithm results significantly higher than the other two, pointing to issues in the ghost suppression mechanism of the algorithm, which needs to be revised. Both efficiency and fraction of ghosts are however consistent in different stations for every algorithm.

The results of the study in different quality categories show that restricting the accepted trigger primitive quality lowers both efficiency and fraction of ghosts. An optimal trade-off between trigger efficiency and fraction of ghost has been identified as the one where trigger segments are reconstructed using at least 4 hits from contiguous DT detection layers. Further studies, based on the reconstruction of full muon trigger tracks, are anyhow needed to confirm this finding.

Finally, the quality of ghost triggers was compared with the one of the trigger segment built using most DT hits. The study was performed to identify the mechanisms that dominate the generation of ghosts for the various algorithm, to pinpoint the cases where the ghost suppression logic could be improved.

Bibliography

[1] S. Chatrchyan *et al.* [CMS Collaboration], "The CMS Experiment at the CERN LHC," JINST **3** (2008) S08004.

[2] A. M. Sirunyan *et al.* [CMS Collaboration], "Performance of the CMS muon detector and muon reconstruction with proton-proton collisions at $\sqrt{s} = 13$ TeV," JINST **13** (2018) no.06, P06015

[3] V. Khachatryan *et al.* [CMS Collaboration], "The CMS trigger system," JINST **12** (2017) no.01, P01020

[4] Tapper, A and Acosta, Darin, "CMS Technical Design Report for the Level-1 Trigger Upgrade," CERN-LHCC-2013-011, CMS-TDR-12

[5] M. De Giorgi *et al.*, "Test results of the ASIC front end trigger prototypes for the muon barrel detector of CMS at LHC," Nucl. Instrum. Meth. A **438** (1999) 302.

[6] G. Apollinari, I. Béjar Alonso, O. Brüning, P. Fessia, M. Lamont, L. Rossi and L. Tavian, "High-Luminosity Large Hadron Collider (HL-LHC) : Technical Design Report V. 0.1," CERN Yellow Rep. Monogr. **4** (2017) 1.

[7] The CMS Collaboration, "The Phase-2 Upgrade of the CMS Muon Detectors," CERN-LHCC-2017-012. CMS-TDR-016

[8] D. Contardo, M. Klute, J. Mans, L. Silvestris and J. Butler, "Technical Proposal for the Phase-II Upgrade of the CMS Detector," CERN-LHCC-2015-010, LHCC-P-008, CMS-TDR-15-02.

[9] S. G. López [CMS Muon Group], "A firmware oriented trigger algorithm for CMS Drift Tubes in HL-LHC"

[10] N. Pozzobon, P. Zotto and F. Montecassiano, "A Proposal for the Upgrade of the Muon Drift Tubes Trigger for the CMS Experiment at the HL-LHC," EPJ Web Conf. **127** (2016) 00012.